AGU PUBLICATIONS

Tectonics

RESEARCH ARTICLE
10.1002/2013TC003483

**Key Points:**
- AMS data support the existence of the New England oroclines
- Data show first-order consistency between structural trend and magnetic fabric
- The Hastings Block shows a more complex deformational history

**Correspondence to:**
T. Mochales,
taniamochales@gmail.com

**Citation:**
Mochales, T., G. Rosenbaum, F. Speranza, and S. A. Pisarevsky (2014), Unraveling the geometry of the New England oroclines (eastern Australia): Constraints from magnetic fabrics, *Tectonics*, *33*, doi:10.1002/2013TC003483.

Received 18 NOV 2013
Accepted 13 OCT 2014
Accepted article online 16 OCT 2014

# Unraveling the geometry of the New England oroclines (eastern Australia): Constraints from magnetic fabrics

**Tania Mochales[1,2], Gideon Rosenbaum[1], Fabio Speranza[2], and Sergei A. Pisarevsky[3,4]**

[1]School of Earth Sciences, University of Queensland, Brisbane, Queensland, Australia, [2]Istituto Nazionale di Geofisica e Vulcanologia, Rome, Italy, [3]School of Earth and Environment, University of Western Australia, Crawley, Western Australia, Australia, [4]ARC Centre of Excellence for Core to Crust Fluid Systems and The Institute for Geoscience Research, Department of Applied Geology, Curtin University, Perth, Western Australia, Australia

**Abstract** The southern New England Orogen (NEO) in eastern Australia is characterized by tight curvatures (oroclines), but the exact geometry of the oroclines and their kinematic evolution are controversial. Here we present new data on the anisotropy of magnetic susceptibility (AMS), which provide a petrofabric proxy for the finite strain associated with the oroclines. We focus on a series of preoroclinal Devonian-Carboniferous fore-arc basin rocks, which are aligned parallel to the oroclinal structure, and by examining structural domains, we test whether or not the magnetic fabric is consistent with the strain axes. AMS data show a first-order consistency with the shape of the oroclines, characterized, in most of structural domains, by subparallelism between magnetic lineations, "structural axis" and bedding. With the exception of the Gresford and west Hastings domains, our results are relatively consistent with the existence of the Manning and Nambucca (Hastings) Oroclines. Reconstruction of magnetic lineations to a prerotation (i.e., pre–late Carboniferous) stage, considering available paleomagnetic results, yields a consistent and rather rectilinear NE-SW predeformation fore-arc basin. This supports the validity of AMS as a strain proxy in complex orogens, such as the NEO. In the Hastings Block, magnetic lineations are suborthogonal to bedding, possibly indicating a different deformational history with respect to the rest of the NEO.

## 1. Introduction

The formation of curved orogenic belts (oroclines) and associated vertical-axis block rotations is commonly attributed to overriding-plate deformation in convergent margins [*Rosenbaum and Lister*, 2004; *Cifelli et al*., 2007; *Capitanio et al*., 2011a; *Rosenbaum*, 2014]. Oroclines have traditionally been defined as originally near-linear orogenic belts, which were subsequently subjected to bending [*Carey*, 1955]. Numerous studies have addressed the possible mechanisms associated with oroclinal bending [*Marshak*, 2004; *Sussman and Weil*, 2004; *Van der Voo*, 2004; *Yonkee and Weil*, 2010; *Johnston et al*., 2013], but there are still many uncertainties regarding the three-dimensional structure and the origin of oroclines. One place where the nature and origin of such structures are particularly debated is the New England Orogen (NEO) of eastern Australia (Figure 1), where a complex oroclinal structure involving multiple orogenic curvatures has been documented [e.g., *Cawood and Leitch*, 1985; *Korsch and Harrington*, 1987; *Cawood et al*., 2011a; *Glen and Roberts*, 2012; *Rosenbaum*, 2012b; *Rosenbaum et al*., 2012].

The structure of the New England oroclines is characterized by four major curvatures (Figure 1). In the northern part, the Texas (TX) and Coffs Harbour (CH) Oroclines are relatively well documented and expressed by the curvature of the structural fabrics [*Korsch*, 1981; *Lennox and Flood*, 1997; *Li et al*., 2012]. The oroclines in the southern part include the Manning (MN) [*Korsch and Harrington*, 1987; *Cawood et al*., 2011a; *Li and Rosenbaum*, 2014a, 2014b] and Nambucca/Hastings (NB) Oroclines [*Rosenbaum*, 2010; *Glen and Roberts*, 2012; *Rosenbaum*, 2012a, 2012b], but their exact structure is still controversial [*Li and Rosenbaum*, 2014a, 2014b; *Offler et al*., 2014].

The formation of the New England oroclines has been explained by a number of alternative mechanisms. In some models [*Murray et al*., 1987; *Offler and Foster*, 2008], it has been suggested that oroclinal bending occurred in response to dextral strike-slip faulting (Figure 2a), but such a model can only explain the Z-shaped structure of the Texas and Coffs Harbour Oroclines. *Cawood et al*. [2011a] assumed a progressive

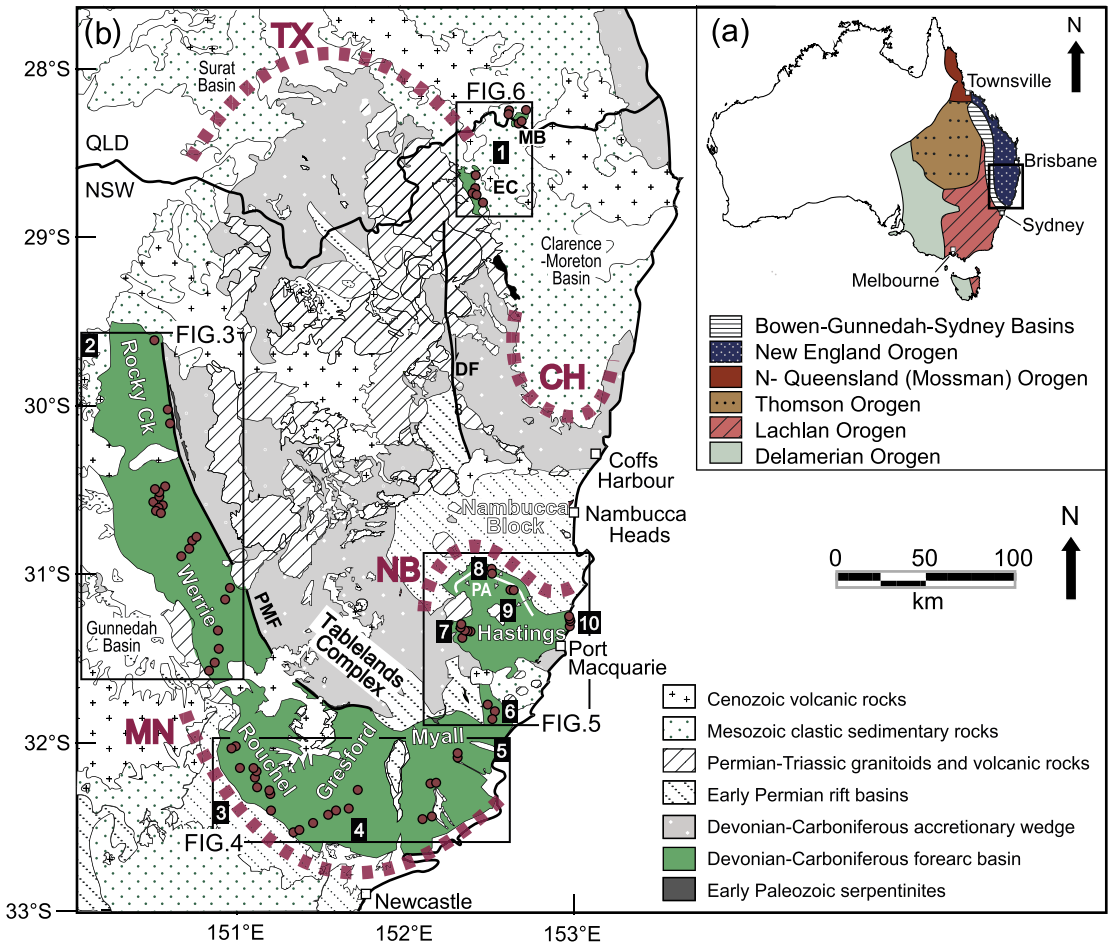


**Figure 1.** (a) Location map of the southern NEO within the Tasmanides of eastern Australia. (b) Geological map of the southern NEO modified from *Rosenbaum et al.* [2012]: DF – Demon Fault; PMF – Peel Manning Fault; EC – Emu Creek; MB – Mount Barney; PA – Parrabel anticline; Oroclines discussed in this work are: CH – Coffs Harbour; TX – Texas; MN – Manning; NB – Nambucca. Structural domains are (1) Emu Creek-Mount Barney, (2) northern Tamworth, (3) Rouchel, (4) Gresford, (5) Myall, (6) South Hastings, (7) West Hastings, (8) North Hastings, (9) NE Hastings, and (10) East Hastings. Circles indicate sampling sites.

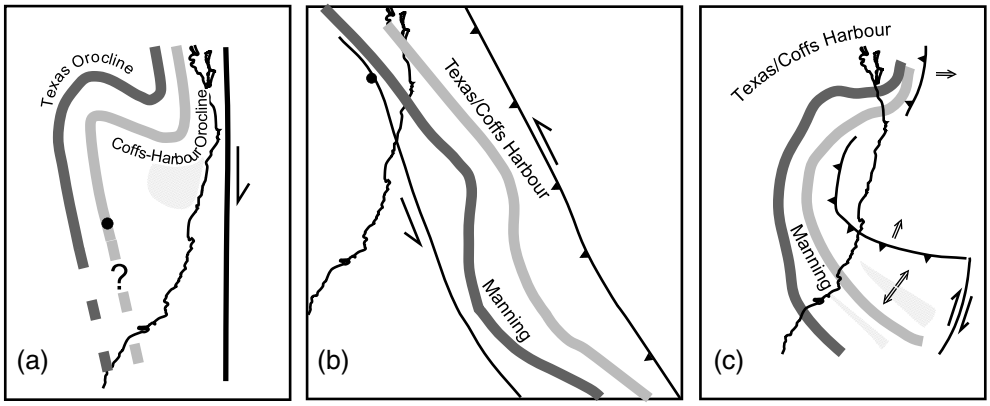


**Figure 2.** Alternative models for the origin of the New England oroclines (modified after *Rosenbaum* [2012a]). (a) Dextral strike-slip faulting [*Offler and Foster*, 2008]. (b) Progressive northward (sinistral) translation and buckling [*Cawood et al.*, 2011a]. (c) Combination of a curvature generated by subduction rollback, followed by contractional and/or transpressional deformation [*Rosenbaum et al.*, 2012].

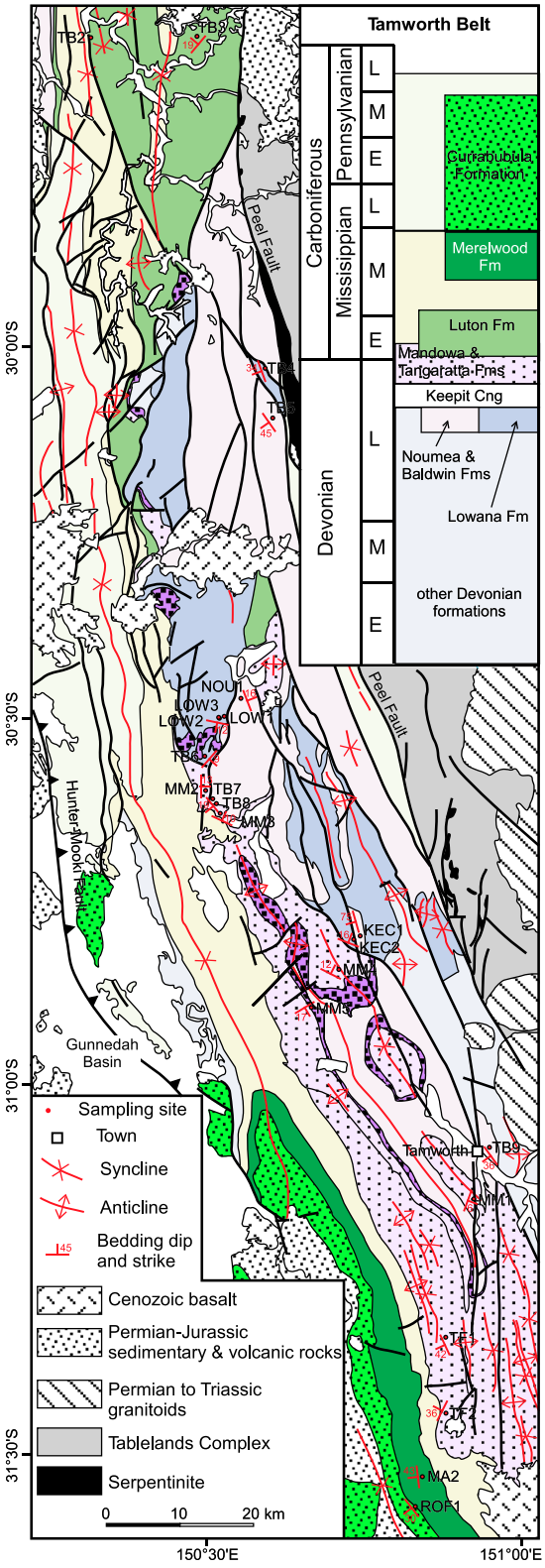


**Figure 3.** Geological map of the northern Tamworth Belt (Werrie and Rocky Creek Blocks) showing major faults, folds, bedding orientations, and sampling sites. The map is modified after *Stroud and Brown* [1998], *Brown et al.* [1992], and *Offenberg* [1971].

northward sinistral translation and buckling of the southern segment of a Devonian-Carboniferous subduction system against the northern segment (Figure 2b). *Rosenbaum et al.* [2012] introduced a more complicated "four-orocline" model, involving the formation of an early curvature by subduction rollback, followed by contractional and/or transpressional deformation that refolded and tightened existing curvatures (Figure 2c).

One of the major hurdles in unraveling the tectonic origin of the New England oroclines is the relatively poor understanding of the exact geometry of the Manning and Nambucca/Hastings Oroclines. The Manning Orocline is inferred from the curved arrangement of Devonian-Carboniferous fore-arc basin blocks (Werrie, Rouchel, Gresford, Myall, and Hastings, Figure 1), which have supposedly experienced vertical-axis rotations and sinistral transpression [*Geeve et al.*, 2002; *Klootwijk*, 2009; *Cawood et al.*, 2011a]. In addition, the map-view curved pattern of early Paleozoic serpentinites [*Wellman*, 1990] and early Permian granitoids [*Rosenbaum et al.*, 2012] is consistent with the geometry of these oroclines. However, direct observations from the hinge of the Manning Orocline, as reflected in the curvature of bedding and/or structural fabrics, are more ambiguous [*Collins*, 1991; *Dirks et al.*, 1992; *Li and Rosenbaum*, 2014a, 2014b]. This led some authors to argue that the Manning Orocline does not exist [*Offler and Foster*, 2008; *Lennox et al.*, 2013; *Offler et al.*, 2014].

In the absence of unambiguous field observations supporting the oroclinal structure (e.g., see inconsistent bedding orientations in Figures 3–6), the controversy on the exact geometry of the New England oroclines could be addressed by investigation of tectonically induced petrofabrics through the analysis of the anisotropy of magnetic susceptibility (AMS) [*Hrouda*, 1982; *Rochette et al.*, 1992; *Martín-Hernández et al.*, 2004]. AMS provides an effective method for describing elements of deformation, especially in rocks that do not show classical strain markers [*Graham*, 1966; *Borradaile*, 1988; *Speranza et al.*, 1997]. The magnetic fabric is expressed as a susceptibility ellipsoid defined by the length and orientation of the main spatial axes $K_{max} \geq K_{int} \geq K_{min}$. If paramagnetic minerals dominate the magnetic susceptibility, this ellipsoid is comparable to the finite strain ellipsoid and allows assessing the degree of

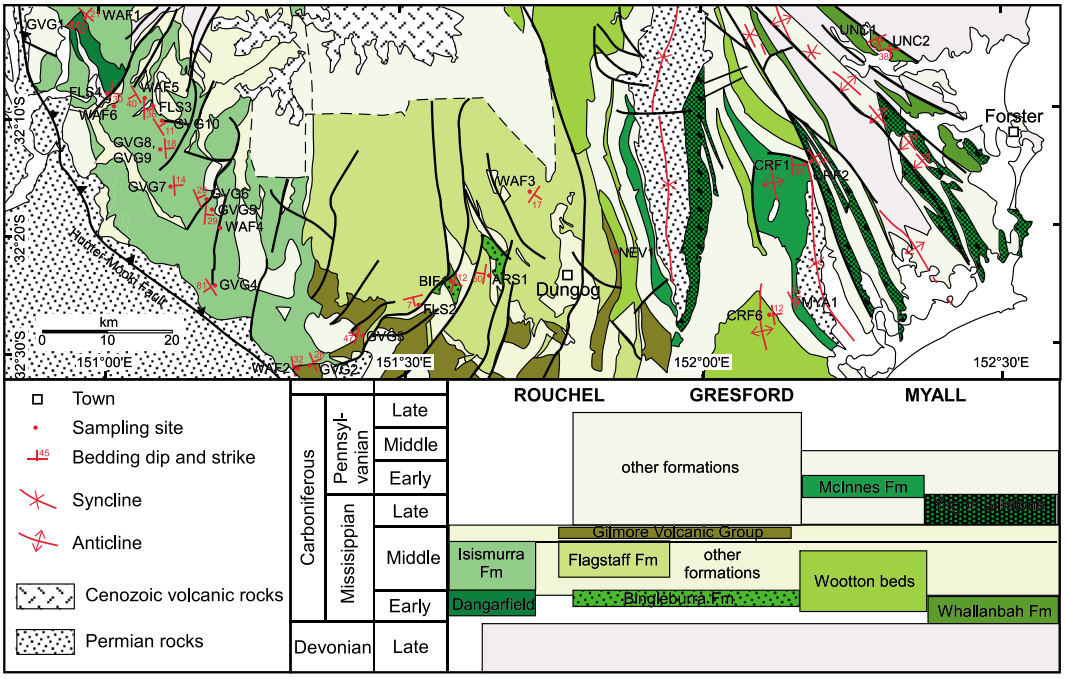


**Figure 4.** Geological map of the Rouchel, Gresford, and Myall Blocks, showing major structures and sampling sites (modified after *Glen and Roberts* [2012]).

correspondence between the mechanical and magnetic processes [*Rochette*, 1987; *Housen and Van der Pluijm*, 1991]. In compressional settings, folding usually controls the magnetic fabric and the axes of maximum susceptibility ($K_{max}$) are generally parallel to fold axes [*Lowrie and Hirt*, 1987; *Aubourg et al*., 2010; *Sagnotti et al*., 1998; *Parés and van der Pluijm*, 2002]. On the other hand, the minimum susceptibility axes ($K_{min}$) commonly cluster around the pole of bedding or cleavage planes.

The only previous attempt to use an AMS analysis for understanding the structure of the New England oroclines was done by *Aubourg et al*. [2004], who presented AMS data from Carboniferous and early Permian rocks in the area of the Texas and Coffs Harbour Oroclines. Their results have shown a general consistency between the magnetic fabrics and the oroclinal structure. However, the Manning and Nambucca/Hastings Oroclines have hitherto not been studied by means of AMS analysis.

The aim of this paper is to test whether the magnetic fabric in the southern NEO is consistent with the proposed oroclinal structure, particularly of the controversial Manning and Nambucca/Hastings Oroclines. We have focused on relatively mildly deformed Devonian-Carboniferous metasedimentary successions deposited in the fore-arc basin, which exhibit a wide range of lithologies suitable for AMS analysis (e.g., fine-grained siltstones and claystones). Accordingly, we were able to determine the preferred orientations of the AMS ellipsoid for the variety of magnetic carriers and to demonstrate their relationships to the oroclinal structure.

## 2. Geological Setting

The NEO is the easternmost and youngest segment of the Tasmanides [*Cawood*, 2005; *Glen*, 2005], stretching for ~2000 km between Townsville and Newcastle (Figure 1). Most rocks in the NEO belong to a late Paleozoic convergent plate margin and associated volcanic arc, fore-arc basin, and accretionary wedge complex [*Leitch*, 1974; *Murray et al*., 1987]. Orogenesis continued until the Triassic in a convergent continental margin dominated by a west dipping subduction zone [*Leitch*, 1974]. In the southern part of the orogen, between Brisbane and Newcastle, most of the exposed Paleozoic rocks are Devonian and Carboniferous successions, which were accumulated in the fore-arc region (accretionary complex and fore-arc basin). Evidence for the coeval continental arc is found farther west, but most of these rocks are covered by younger sedimentary rocks and/or overthrust by the fore-arc basin units (Figure 1). Rocks of the Devonian-Carboniferous fore-arc basin (Tamworth Belt and correlative blocks) are separated from the accretionary complex (Tablelands Complex) by a

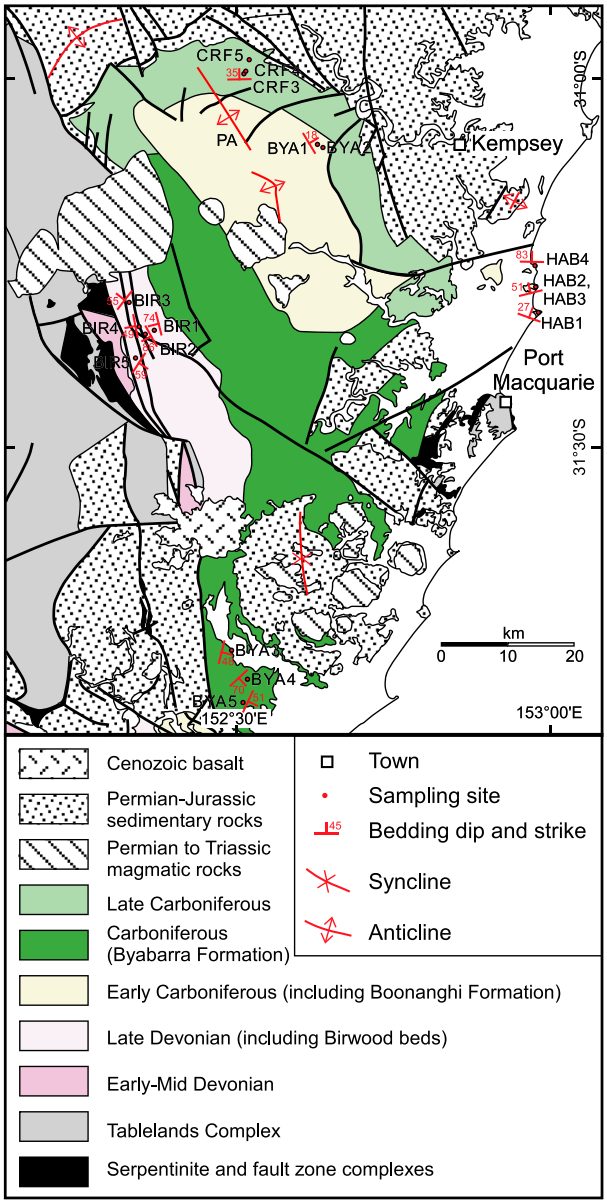


**Figure 5.** Geological map of the Hastings Block, showing major structures and sampling sites. The map is modified after *Gilligan et al.* [1987] with additional elements from *Lennox et al.* [2013]. PA, Parrabel Anticline.

tectonic contact, the Peel-Manning Fault System (PMF, Figures 1 and 3), along which there are exposures of serpentinites and high-pressure rocks derived from an early Paleozoic ophiolitic mélange [*Aitchison et al.*, 1994]. The exposed Devonian-Carboniferous fore-arc basin rocks in the NEO have been subjected to low-grade burial metamorphism at zeolite and prehnite-pumpellyite facies conditions [*Offler et al.*, 1997]. Within the accretionary complex units, metamorphic conditions range from prehnite-pumpellyite to greenschist facies [*Binns et al.*, 1967; *Korsch*, 1978], with local occurrences of high-grade (amphibolite-facies) metamorphism [*Stephenson and Hensel*, 1982; *Craven et al.*, 2012].

Younger rocks in the study area include Permian to Triassic magmatic and sedimentary rocks, which are overlain by younger Mesozoic sedimentary successions and Cenozoic basalts (Figure 1). Early Permian rocks include S-type granitoids and clastic sedimentary successions, which have possibly been deposited in a back-arc extensional setting [*Cawood et al.*, 2011b; *Rosenbaum et al.*, 2012]. In contrast, during the middle-late Permian (~265 Ma to ~230 Ma), tectonic activity throughout the NEO was dominated by contraction, normally referred to as the Hunter-Bowen phase of deformation [*Holcombe et al.*, 1997]. Magmatic activity during this period mainly involved the emplacement of I-type granitoids and calc-alkaline volcanism [*Shaw and Flood*, 1981; *Holcombe et al.*, 1997].

### 2.1. Tectonostratigraphic Setting

This study focuses on the Devonian-Carboniferous fore-arc basin rocks, which are best exposed in the Tamworth Belt. The Tamworth Belt (in a broad sense) occurs in an approximately North-South elongated segment that runs along the western margin of the southern NEO (Figure 3) and in three displaced blocks at the southernmost part of the fold belt (Rouchel, Gresford, and Myall Blocks; Figure 4). Other fore-arc basin blocks that are likely correlated with the Tamworth Belt are the Hastings Block (Figure 5) and the relatively small exposures of Emu Creek Block and Mount Barney inlier in the area of the Texas/Coffs Harbour Oroclines (Figure 6).

The stratigraphy of the Tamworth Belt consists of two major sedimentary successions. In the northern Tamworth Belt (Werrie and Rocky Creek Blocks; Figures 1 and 3), a succession of Devonian rocks, sometimes referred to as the Gamilaroi Terrane [*Flood and Aitchison*, 1992], occurs in the east and may represent an allochthonous terrane accreted to the continent by late Devonian or middle Carboniferous [*Powell et al.*, 1990; *Aitchison et al.*, 1992]. The succession farther west is made of Late Devonian to Carboniferous strata,

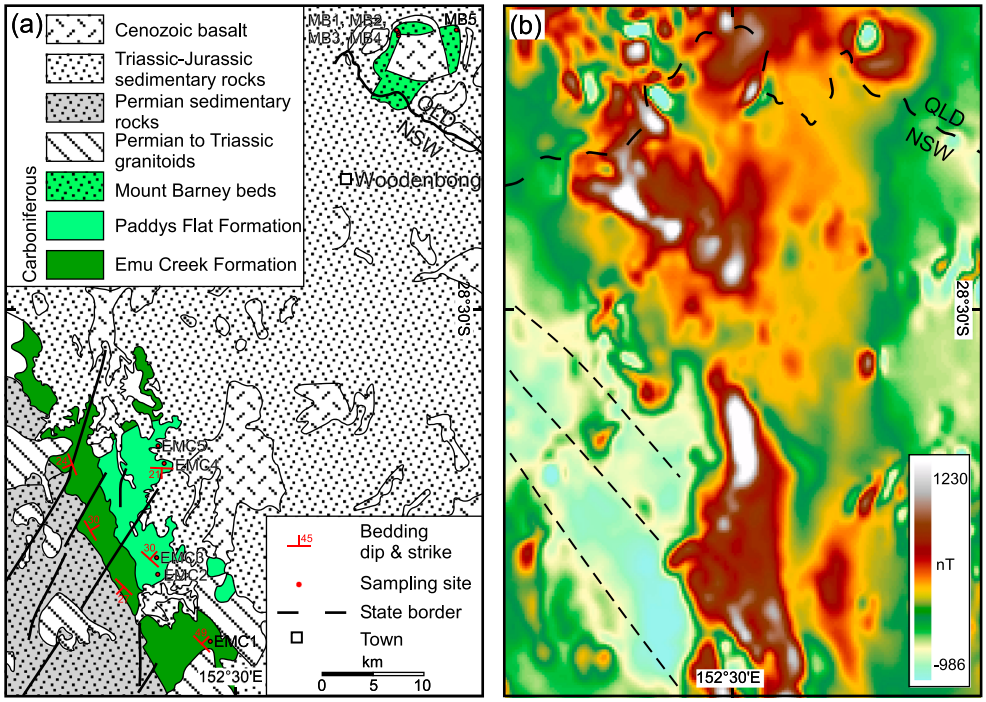


**Figure 6.** (a) Geological map of the Emu Creek Block and Mount Barney inlier showing major structures and sampling sites. The map is modified after *Whitaker et al.* [1980] and *Hoy et al.* [2014]. (b) Gridded reduced to pole aeromagnetic image of the study area (brown = positive anomalies). NW-SE low magnetic structures are recognized in Emu Creek, whereas high-magnetization basalts mask the structural grain in the area of Mount Barney.

deposited in a shelf environment east of the volcanic arc and west of the deeper water Tablelands Complex [*Roberts and Engel*, 1987].

The structure of the Werrie and Rocky Creek Blocks is dominated by faults and folds that run parallel to the dominant N to NNW structural grain (with local deflections, Figure 3). The onset of deformation and low-grade metamorphism may have occurred shortly after the termination of sedimentation, at circa 305 Ma, during a short (<5 Myr) episode of contractional tectonism [*Cawood et al.*, 2011b]. The majority of the structures, however, seem to be associated with the younger Hunter-Bowen phase of deformation that took place in the late Permian and Triassic (265–230 Ma). Associated with this deformation is the west vergent Hunter-Mooki thrust, which marks the western boundary of the fore-arc basin (Figure 3) and juxtaposes rocks of the Tamworth Belt on top of younger (Permo-Triassic) sedimentary rocks of the Gunnedah Basin [*Korsch et al.*, 2009]. The eastern boundary of the Werrie and Rocky Creek Blocks, the Peel-Manning Fault System, is a higher angle fault, which was likely subjected to a prolonged tectonic history involving both strike-slip and reverse movements [*Offler and Williams*, 1987]. The reverse component was likely relatively minor, based on the absence of a substantial metamorphic contrast between the Tamworth Belt and Tablelands Complex rocks from both sides of the fault zone [*Blake and Murchey*, 1988].

The structure of the Tamworth Belt in the southern blocks (Rouchel, Gresford, and Myall Blocks) is associated with an early phase of approximately North-South oriented folds, superimposed by later deformation that involved thrusting, sinistral strike-slip faulting and folding [*Collins*, 1991; *Glen and Roberts*, 2012]. Folds interference gave rise to dome-and-basin structures. In this area, the two major fault systems of the Hunter-Mooki and Peel-Manning fault zones form an arcuate shape that follows the southern and northern boundaries of the fore-arc basin, respectively (Figures 1, 3, and 4).

North of the Myall Block, the possible continuation of the Tamworth Belt is more complex (Figure 1). Late Devonian to Carboniferous fore-arc basin rocks are exposed in the Hastings Block (Figure 5), but its stratigraphy is not continuous with the Tamworth Belt succession [*Roberts et al.*, 1995]. It is possible that this is a displaced block of the Tamworth Belt [*Scheibner*, 1976; *Leitch*, 1980; *Cawood*, 1982; *Roberts et al.*, 1993;

*Glen and Roberts*, 2012], but its exact origin and structural evolution are debated [*Schmidt et al*., 1994; *Cawood et al*., 2011a; *Glen and Roberts*, 2012]. In addition, major stratigraphic and structural differences between the northern and southern parts of the Hastings Block [*Roberts et al*., 1995] suggest that the block is internally deformed and may not represent a single terrane. The deformation history of the Hastings Block is relatively poorly understood. The most prominent structure is the NW-SE Parrabel anticline (PA, Figure 5), which is a doubly plunging fold that deforms older folds and cleavage [*Lennox and Roberts*, 1988]. Faults are predominantly oriented NNW-SSE. According to *Lennox et al*. [2013], deformation involved three generations of faulting.

North of latitude 29.5°S, the Tamworth Belt is not exposed but is thought to continue in the subsurface under the younger sedimentary cover [*Wartenberg et al*., 2003]. Carboniferous fore-arc basin rocks (Emu Creek Formation) are found in the Emu Creek Block [*Cawood and Leitch*, 1985; *Cross et al*., 1987; *Hoy et al*., 2014], which is located in the eastern limb of the Texas Orocline (Figures 1 and 6). Bedding orientations and macroscopic folds are generally oriented NW-SE, parallel to the limb of the orocline [*Hoy et al*., 2014]. A relatively small exposure of Carboniferous sedimentary rocks, possibly correlative to the Emu Creek Formation, is present in the Mount Barney inlier [*Murray et al*., 1981; *Rosenbaum*, 2012b], immediately north of the Queensland/NSW state border (Figure 6). However, due to the limited exposure, the stratigraphic and structural relationships of the Mount Barney inlier with the rest of the fore-arc basin rocks are relatively poorly understood.

### 2.2. The Oroclinal Structure and Paleomagnetic Constraints

The oroclinal structure, particularly the Texas-Coffs Harbour Orocline, is clearly visible in aeromagnetic and gravity images and is featured by the curvature of bedding, structural fabrics, and magnetic fabrics [*Korsch*, 1981; *Lennox and Flood*, 1997; *Aubourg et al*., 2004; *Li et al*., 2012]. The structure of the Manning and Nambucca/Hastings Oroclines is delineated by the curvature of serpentinites (possibly the southeastward continuation of the Peel-Manning fault zone) and early Permian granitoids [*Rosenbaum*, 2012b; *Rosenbaum et al*., 2012]. However, the question whether or not these oroclines exist remains controversial [e.g., *Offler et al*., 2014; *Li and Rosenbaum*, 2014a, 2014b].

The timing of oroclinal bending in the Texas/Coffs Harbour Orocline is constrained to the early-middle Permian (300–260 Ma). *Rosenbaum et al*. [2012] have shown that early Permian (298–288 Ma) granitoids are curved around the oroclinal structure, indicating that the oroclines have been formed during or after granite emplacement. Recent studies [*Rosenbaum et al*., 2012; *Li et al*., 2014; *Shaanan et al*., 2014] have considered that the first stage of oroclinal bending occurred during back-arc extension at 300–285 Ma, and was followed by the second stage at 275–265 Ma. Oroclinal bending was concluded prior to the emplacement of the Late Permian to Triassic (260–220 Ma) New England Batholith, which crosscut the oroclinal structure [*Offler and Foster*, 2008; *Rosenbaum et al*., 2012]. A number of authors [e.g., *Korsch and Harrington*, 1987; *Offler and Foster*, 2008; *Cawood et al*., 2011a] proposed that the major phase of oroclinal bending occurred at ~280–260 Ma, but an earlier phase of rotation (prior to ~293 Ma) has been proposed by *Aubourg et al*. [2004] based on paleomagnetic data from the 293 Ma Alum Rock ignimbrite. According to their data, a ~40° clockwise rotation occurred before 293 Ma and a further rotation of ~80° during subsequent deformation. This interpretation was based on the comparison of the Alum Rock paleomagnetic pole with the Apparent Polar Wander Path (APWP) of *Klootwijk and Giddings* [1993]. This APWP, however, has been disputed [e.g., *Geeve et al*., 2002; *McElhinny et al*., 2003, and references therein]. Paleomagnetic data from the Coffs Harbour Orocline [*Klootwijk et al*., 1993] indicate a reverse polarity, likely associated with the late Carboniferous to early Permian Kiaman superchron. The exact timing of this overprint is unknown.

In the area of the Manning Orocline, paleomagnetic data by *Geeve et al*. [2002] have shown that the Rouchel, Gresford, and Myall Blocks were subjected to counterclockwise rotations (80°, 80°, and 120°, respectively) relative to cratonic Australia. According to these authors, the rotations were completed prior to the late Asselian (~296 Ma). Paleomagnetic data from the Hastings Block are ambiguous and were interpreted to indicate 130° clockwise or 230° counterclockwise rotations [*Schmidt et al*., 1994], or 150° counterclockwise rotation [*Klootwijk*, 2009]. *Cawood et al*. [2011a] suggested that these apparent rotations, especially in view of high paleomagnetic inclinations (high paleolatitudes), could at least partly result from a long distance movement across paleomeridians. These authors concluded that the number of coeval paleopoles from the different rotated blocks is currently insufficient.

## 3. Sampling and Laboratory Procedures

In order to study magnetic fabrics throughout the southern NEO, 78 sites were hand sampled during three surveys to the Tamworth Belt and correlative blocks. In average, nine oriented samples were collected in each site. Sites were selected to represent a broad coverage around the Texas, Coffs Harbour, Manning, and Nambucca Oroclines (Figure 1 and Table 1). Twenty-three sites were sampled in the northern Tamworth Belt (Figure 3), 14 sites in the Rouchel Block, 7 sites in the Gresford Block, 7 sites in the Myall Block (Figure 4), and 17 sites in the Hastings Block (Figures 5). Ten sites were sampled in the area of the Texas/Coffs Harbour Oroclines (five in the Emu Creek Block and five in the Mount Barney inlier, Figure 6). Sampled lithologies comprise low-grade and unmetamorphosed mudstones, siltstones and sandstones with variable content of turbidites and volcanoclastic material, and igneous rocks (Table 1). In order to optimize the AMS results, preference has been given to the fine-grained rocks (in case of clastic rocks), because magnetic fabric is normally well preserved in clayey materials. In total, we collected 245 oriented samples of Devonian and Carboniferous rocks and prepared 798 standard specimens for AMS studies. The dimensions of the standard specimens are cubes of 2 cm (height) × 2 cm (length) × 2 cm (width) with a volume of approximately 8 $cm^3$.

The axis of maximum susceptibility, $K_{max}$, is commonly parallel to the maximum elongation direction of the strain ellipsoid [*Hrouda*, 1982]. $K_{max}$ is contained within the bedding or cleavage planes and is named the magnetic lineation. Similarly, the axis of minimum susceptibility, $K_{min}$, is the pole to the magnetic foliation. The magnitudes and orientations of the three principal axes can be calculated by statistical procedures [*Jelinek*, 1981]. The corrected degree of anisotropy ($P'$) and the shape parameter ($T$) are scalar parameters that characterize the ellipsoid. $P$ is the degree of anisotropy, which can be related to magnetic mineral type, amount, and orientation [*Nagata*, 1961], and $P'$ is the corrected anisotropy degree, as proposed by *Jelinek* [1981]. $T$ represents the shape of the susceptibility ellipsoid, which can be oblate ($T > 0$) or prolate ($T < 0$) [*Jelinek*, 1981].

AMS analyses were performed at the University of Zaragoza (Geotransfer Research Group, Spain). Analyses were done with a susceptibility bridge (KLY-3S, AGICO) at 875 Hz and field intensity of 300 $Am^{-1}$. We measured 61 samples, representative of the rock types in the data set at room temperature and, after immersion in liquid nitrogen for 90 minutes, at low temperature (77 K). To prevent heating, the samples have been again submerged in nitrogen for 10 min between each measurement. Paramagnetic susceptibility at low temperatures increases by a factor of 3 to 5 at room temperature [*Parés and van der Pluijm*, 2002], with the magnitude of $K_{max}$ increasing more than the magnitude of $K_{min}$.

Directional analysis of site means ($K_{max}$ and $K_{min}$) has been done using the *Jelinek* [1981] statistics. We have also calculated the Bingham statistics for $K_{min}$ distribution, which is an adequate method when dispersion of directions is expected to have an antipodal symmetry. The statistical model of Bingham (1964) describes populations of points on a sphere that may array in girdles with an axial symmetry, as occurs for $K_{min}$ distribution in a fold. Thus, the Bingham's statistics was used to determine the girdle of the $K_{min}$ scattering and its pole that corresponds to the "structural axis."

## 4. Results

### 4.1. Magnetic Properties

The bulk susceptibility ($\kappa$) of the studied rocks varies with lithology (Table 1). Low susceptibilities (ranging from 50 to 500 × $10^{-6}$ International System (S.I.)) are characteristic for 73% of the sedimentary rocks, whereas rocks with variable contents of volcaniclastic material (e.g., from the Isismurra Formation and Gilmore Volcanic Group) are more magnetic (100 to 900 × $10^{-6}$ S.I.). Magmatic rocks (e.g., from the Gilmore Volcanic Group) are highly magnetic with susceptibilities up to 7700 × $10^{-6}$ S.I. (Table 1 and Figure 7c). The degree of anisotropy ranges from 1.003 to 1.12 with mean values ($P' = 1.023$) that indicates a higher strain in comparison with clastic sedimentary rocks from previous studies [*Aubourg et al.*, 2004] (see Figure 7a). The shape parameter ($T$) ranges from oblate to prolate (0.839 to −0.552), but 77.2% of the samples are in the oblate domain (Figure 7b).

Paramagnetic minerals dominate the magnetic susceptibility [*Rochette*, 1987; *Housen and van der Pluijm*, 1991; *Bouchez*, 1997], as shown in Figure 7c, although small quantities of ferromagnetic minerals can also contribute to the AMS. Therefore, quantification of the ferromagnetic/paramagnetic ratio must be assessed.

**Table 1.** Field Data and Magnetic Fabric Parameters[a]

| Structural Domain | Label | Latitude | Longitude | *n/N* | Fm | Lithology | DipAz | Dip |
|---|---|---|---|---|---|---|---|---|
| Tamworth | TB2 | −29.579670 | 150.323194 | 5/5 | Luton Fm | Congomerate, Microconglomerate | | |
| Tamworth | TB3 | −29.580065 | 150.490065 | 7/7 | Luton Fm | Clays/Volcanoclastics | 310 | 19 |
| Tamworth | TB4 | −30.029732 | 150.593196 | 6/6 | Lowana Fm | Silt/Sandstone | 250 | 34 |
| Tamworth | TB5 | −30.099369 | 150.604539 | 6/6 | Noumea Fm | Green-black siltstone and mudstone | 235 | 45 |
| Tamworth | MM1 | −31.154934 | 150.921192 | 9/9 | Mandowa Mudstone | Low metamorphic slate | 110 | 6 |
| Tamworth | TF1 | −31.341284 | 150.877515 | 9/9 | Tangaratta Fm | Mud/sandstone from turbidite | 245 | 42 |
| Tamworth | TF2 | −31.443020 | 150.878117 | 9/9 | Tangaratta Fm | Mud/sandstone from turbidite | 297 | 36 |
| Tamworth | MA2 | −31.528894 | 150.841053 | 8/8 | Merlewood Andesite | Arc columnar andesite | 263 | 43 |
| Tamworth | ROF1 | −31.568712 | 150.829157 | 9/9 | Currabubula Formation | Volcanoclastic ignimbrite | 232 | 30 |
| Tamworth | NOU1 | −30.478219 | 150.553051 | 10/10 | Noumea Fm | Green-black volcanoclastic sandstone | 69 | 16 |
| Tamworth | LOW1 | −30.500919 | 150.528233 | 9/10 | Lowana Fm | Green-black volcanoclastic silt/sandstone | 111 | 22 |
| Tamworth | LOW2 | −30.503413 | 150.519511 | 11/11 | Lowana Fm | Siltstone/Sandstone volcanoclastics | 357 | 13 |
| Tamworth | LOW3 | −30.502203 | 150.518665 | 10/10 | Lowana Fm | Siltstone | 192 | 12 |
| Tamworth | TB6 | −30.554556 | 150.498372 | 9/9 | Lowana Fm | Mudstone arenite, mudstone, thin sandstone | 131 | 9 |
| Tamworth | MM2 | −30.599847 | 150.497552 | 9/9 | Mandowa Mudstone | Mudstone, thin sandstone | 90 | 13 |
| Tamworth | TB7 | −30.612695 | 150.509920 | 9/9 | Keepit Conglomerate | Alternance coarse sandstone and siltstone | 165 | 20 |
| Tamworth | TB8 | −30.619155 | 150.514849 | 8/8 | Keepit Conglomerate | Green-black sandstone | 231 | 19 |
| Tamworth | MM3 | −30.632109 | 150.520810 | 9/9 | Mandowa Mudstone | Dark gray mudstone, thin sandstone | 25 | 10 |
| Tamworth | KEC1 | −30.798478 | 150.741066 | 10/10 | Noumea Fm | Alternance of sandstone and polymictic microconglomerate | 254 | 75 |
| Tamworth | KEC2 | −30.803938 | 150.730980 | 11/11 | Lowana Fm | Shale | 21 | 16 |
| Tamworth | MM4 | −30.844682 | 150.706709 | 9/9 | Mandowa Mudstone | Mudstone, thin sandstone | 27 | 12 |
| Tamworth | MM5 | −30.895258 | 150.663828 | 10/10 | Keepit Conglomerate | Mudstone, thin sandstone | 149 | 17 |
| Tamworth | TB9 | −31.084347 | 150.945569 | 10/10 | Baldwin Fm | Greywake, argillite | 234 | 36 |
| Rouchel | GVG1 | −32.033059 | 150.955012 | 8/8 | Dangarfield Fm | Mudstone | 26 | 22 |
| Rouchel | WAF1 | −32.025435 | 150.975813 | 7/8 | Dangarfield Fm | Siltstone/tuff layering | 42 | 21 |
| Rouchel | GVG4 | −32.407834 | 151.182875 | 9/9 | Isismurra Fm | Andesite | 237 | 81 |
| Rouchel | WAF4 | −32.335947 | 151.204601 | 9/9 | Isismurra Fm | Conglomerate acid tuffs, lithic red-brown siltstones | | |
| Rouchel | GVG5 | −32.302984 | 151.182658 | 9/9 | Isismurra Fm | Volcanoclastic sandstone | 95 | 29 |
| Rouchel | GVG6 | −32.288341 | 151.172783 | 10/10 | Isismurra Fm | Volcanoclastic sandstone | 67 | 20 |
| Rouchel | GVG7 | −32.266269 | 151.115187 | 9/9 | Isismurra Fm | Volcanoclastic sandstone | 86 | 14 |
| Rouchel | GVG8 | −32.214537 | 151.100305 | 9/9 | Isismurra Fm | Volcanoclastic siltstone | 86 | 18 |
| Rouchel | GVG9 | −32.214424 | 151.099942 | 9/9 | Isismurra Fm | Volcanoclastic sandstone | 86 | 18 |
| Rouchel | GVG10 | −32.173824 | 151.100969 | 10/10 | Isismurra Fm | Volcanoclastic sandstone | 58 | 11 |
| Rouchel | FLS3 | −32.152615 | 151.088541 | 8/9 | Isismurra Fm | Red Lavas | 89 | 36 |
| Rouchel | WAF5 | −32.146396 | 151.070452 | 9/9 | Isismurra Fm | Acid tuffs, lithic red-brown siltstones | 240 | 40 |
| Rouchel | WAF6 | −32.151639 | 151.023186 | 9/9 | Isismurra Fm | Volcanoclastic sandstone | | |
| Rouchel | FLS4 | −32.148295 | 151.011543 | 9/9 | Dangarfield Fm | Volcanoclastic sandstone/mudstone | 99 | 30 |
| Gresford | WAF2 | −32.527475 | 151.321295 | 8/8 | Gilmore Volcanic Gp | Sandstone/conglomerate with andesite pebble | 80 | 32 |
| Gresford | WAF3 | −32.283306 | 151.710939 | 4/4 | Flagstaff Fm | Volcanoclastic, lithic sandstone, green tuffaceous sandstone | 124 | 17 |
| Gresford | GVG2 | −32.524039 | 151.345048 | 8/8 | Gilmore Volcanic Gp | Andesite/Ignimbrite | 68 | 28 |
| Gresford | GVG3 | −32.483617 | 151.431054 | 8/8 | Gilmore Volcanic Gp | Red beds/sandstone | 286 | 47 |
| Gresford | FLS2 | −32.438869 | 151.527308 | 8/8 | Flagstaff Fm | Volcanoclastic sandstone/mudstone | 166 | 7 |
| Gresford | BIF1 | −32.408078 | 151.580486 | 9/9 | Bingleburra Fm | Sandstone/blue siltstone | 107 | 12 |
| Gresford | ARS1 | −32.398983 | 151.644121 | 8/8 | Flagstaff Fm | Sandstone volcanoclastics | 279 | 50 |
| Myall | NEV1 | −32.370092 | 151.854996 | 7/8 | Gilmore Volcanic Gp | Andesite | | |
| Myall | CRF1 | −32.247743 | 152.167603 | 9/9 | McInnes Fm | White/red sandstone | 87 | 35 |
| Myall | CRF2 | −32.240769 | 152.181081 | 8/8 | Yagon Siltstone | Mudstone | 56 | 39 |
| Myall | UNC1 | −32.071788 | 152.302839 | 9/9 | Wallanbah Fm | Mudstone alternated with sandstone | 157 | 19 |
| Myall | UNC2 | −32.082610 | 152.318869 | 10/10 | Wallanbah Fm | Sandstone/mudstone/tuff/shale | 178 | 38 |
| Myall | MYA1 | −32.443314 | 152.162534 | 9/9 | McInnes Fm | Alternance sandstone/few siltstone | 61 | 53 |
| Myall | CRF6 | −32.460050 | 152.109752 | 9/9 | Wootton Beds | Lithic sandstone | 81 | 12 |
| East Hastings | HAB1 | −31.311349 | 152.972272 | 8/8 | Boonanghi beds | Sandstone | 20 | 27 |
| East Hastings | HAB2 | −31.278362 | 152.969848 | 8/8 | Boonanghi beds | Mudstone in the sandy sequence | 346 | 51 |
| East Hastings | HAB3 | −31.278939 | 152.972239 | 8/8 | Boonanghi beds | Turbiditic sandstone | 348 | 42 |
| East Hastings | HAB4 | −31.250618 | 152.967534 | 8/8 | Boonanghi beds | Lithic sandstone | 1 | 83 |
| West Hastings | BIR1 | −31.343802 | 152.362332 | 9/9 | Birdwood beds | Sandstone/mudstone/shale | 256 | 74 |
| West Hastings | BIR2 | −31.350228 | 152.349346 | 12/12 | Birdwood beds | Laminated sandstone/mudstone/shale | 241 | 86 |
| West Hastings | BIR3 | −31.305781 | 152.322956 | 10/10 | Birdwood beds | Laminated sandstone/mudstone/shale | 308 | 55 |
| West Hastings | BIR4 | −31.338872 | 152.339957 | 10/10 | Birdwood beds | Green sandstone/mudstone/shale | 259 | 49 |
| West Hastings | BIR5 | −31.383289 | 152.335468 | 8/9 | Birdwood beds | Sandstone/siltstone/shale | 123 | 59 |
| North Hastings | CRF3 | −30.994832 | 152.505187 | 10/10 | Majors Creek Fm | Alternating sandstone/mudstone | 359 | 35 |
| North Hastings | CRF4 | −30.990251 | 152.509111 | 8/8 | Majors Creek Fm | Siltstone/Lithic sandstone | 7 | 27 |
| North Hastings | CRF5 | −30.974628 | 152.514722 | 8/9 | Majors Creek Fm | Lithic sandstone | 111 | 44 |
| NE Hastings | BYA1 | −31.090977 | 152.620860 | 11/11 | Boonanghi beds | Lithic sandstone | 59 | 18 |
| NE Hastings | BYA2 | −31.094547 | 152.630577 | 11/11 | Boonanghi beds | Foliated sandstone/shale | 329 | 17 |
| South Hastings | BYA3 | −31.780252 | 152.491987 | 9/9 | Byabarra Fm | Lithic sandstone/tuff/shale | 104 | 48 |
| South Hastings | BYA4 | −31.819742 | 152.515790 | 7/7 | Byabarra Fm | Lithic mudstone | 137 | 70 |
| South Hastings | BYA5 | −31.850008 | 152.507858 | 9/9 | Byabarra Fm | Lithic sandstone/tuff/shale | 115 | 51 |
| Emu Creek-Mount\ Barney | EMC1 | −28.793120 | 152.473100 | 6/6 | Emu Creek Fm | Mississippian Faunal silt | 45 | 49 |
| Emu Creek-Mount Barney | EMC2 | −28.733317 | 152.420182 | 8/8 | Paddys Flat Fm | Massive sandstone | 113 | 25 |
| Emu Creek-Mount Barney | EMC3 | −28.719585 | 152.419135 | 8/8 | Paddys Flat Fm | Selected mud/siltstone | 42 | 30 |
| Emu Creek-MountBarney | EMC4 | −28.635146 | 152.426918 | 9/9 | Paddys Flat Fm | Sandstone | 182 | 21 |
| Emu Creek-Mount Barney | EMC5 | −28.621750 | 152.421081 | 7/7 | Paddys Flat Fm | Coarse Sandstone | | |
| Emu Creek-Mount Barney | MB1 | −28.259274 | 152.662050 | 9/9 | Mount Barney Beds | Siltstone, mudstone | | |
| Emu Creek-Mount Barney | MB2 | −28.257726 | 152.661961 | 10/10 | Mount Barney Beds | Sandstone, conglomerate, mudstone | | |
| Emu Creek-Mount Barney | MB3 | −28.254849 | 152.661485 | 11/11 | Mount Barney Beds | Sandstone, conglomerate, mudstone | 335 | 44 |
| Emu Creek-Mount Barney | MB4 | −28.250656 | 152.660100 | 8/9 | Mount Barney Beds | Sandstone, conglomerate, mudstone | 85 | 52 |
| Emu Creek-Mount Barney | MB5 | −28.253118 | 152.721846 | 10/10 | Mount Barney Beds | Sandstone, conglomerate, mudstone | 172 | 74 |

[a]The *n/N* is the number of analyzed/measured samples; Fm, Formation; of bedding; DipAz′, Dip′ of the oriented block; spec/site, number of specimen per site; Km, bulk susceptibility; *P′*, degree of anisotropy; *T*, shape of the ellipsoid; Dec $K_{max}$, declination of $K_{max}$; Inc $K_{max}$, inclination of $K_{max}$; Cf. Dec $K_{max}$, confidence angle of declination $K_{max}$; Cf. Inc $K_{max}$, confidence angle of inclination $K_{max}$; $Q_L$, quality lineation; Dec $K_{min}$, declination of $K_{min}$; Inc $K_{min}$, inclination of $K_{max}$; Foliation trend, Foliation Dip; DD Fol., Dip direction of foliation plane.

**Table 1.** (continued)

| DipAz′ | Dip′ | Spec/Site | Km (RT ) | P′ | T | Dec $K_{max}$ | Inc $K_{max}$ | Cf. Dec $K_{max}$ | Cf. Inc $K_{max}$ | $Q_L$ | Dec $K_{min}$ | Inc $K_{min}$ | Foliation Trend | Foliation Dip DD Fol. |
|---|---|---|---|---|---|---|---|---|---|---|---|---|---|---|
| 56 | 36 | 5 | 5.60e−04 | 1,004 | 0.226 | 219 | 8 | 54.2 | 11.5 | 3 | 99 | 75 | 189 | 15 W |
| | | 7 | 3.86e−04 | 1,018 | 0.029 | 349 | 75 | 8.7 | 1.1 | 1 | 98 | 5 | 189 | 86 W |
| 250 | 34 | 6 | 6.83e−05 | 1,015 | 0.309 | 229 | 30 | 26.4 | 3.8 | 2 | 77 | 57 | 167 | 33 W |
| 235 | 45 | 6 | 1.55e−04 | 1,018 | −0.158 | 156 | 14 | 13.5 | 6.7 | 1 | 49 | 50 | 139 | 40 W |
| 73 | 55 | 9 | 3.52e−04 | 1,023 | −0.552 | 341 | 5 | 3.9 | 1.5 | 1 | 247 | 35 | 337 | 55 E |
| 247 | 40 | 9 | 4.41e−04 | 1,016 | 0.165 | 323 | 21 | 7.6 | 4.6 | 1 | 79 | 49 | 169 | 41 W |
| 93 | 84 | 10 | 2.67e−04 | 1,028 | 0.250 | 357 | 6 | 10.6 | 2.8 | 1 | 247 | 74 | 337 | 16 E |
| 15 | 74 | 8 | 2.98e−03 | 1,028 | 0.461 | 357 | 31 | 21.7 | 4.7 | 1 | 248 | 28 | 338 | 62 E |
| 107 | 87 | 9 | 3.72e−04 | 1,010 | 0.495 | 146 | 3 | 12.0 | 3.4 | 1 | 51 | 59 | 141 | 31 W |
| 77 | 11 | 10 | 2.87e−04 | 1,010 | −0.318 | 63 | 9 | 9.3 | 2.0 | 1 | 243 | 81 | 333 | 9 E |
| 111 | 22 | 10 | 4.25e−04 | 1,011 | 0.719 | 132 | 23 | 39.8 | 4.6 | 2 | 297 | 66 | 28 | 23 E |
| 336 | 13 | 10 | 3.27e−04 | 1,022 | 0.519 | 317 | 15 | 9.7 | 2.3 | 1 | 103 | 72 | 193 | 18 W |
| 133 | 13 | 10 | 4.19e−04 | 1,023 | −0.044 | 143 | 14 | 4.5 | 2.5 | 1 | 316 | 75 | 46 | 15 S |
| 136 | 7 | 11 | 3.60e−04 | 1,037 | 0.711 | 172 | 8 | 13.4 | | 1 | 328 | 82 | 53 | 8 S |
| 90 | 13 | 9 | 3.21e−04 | 1,015 | 0.653 | 75 | 13 | 40.3 | 9.7 | 3 | 275 | 76 | 5 | 14 E |
| 169 | 20 | 9 | 2.48e−04 | 1,013 | 0.355 | 162 | 16 | 14.1 | 4.3 | 1 | 357 | 73 | 87 | 17 S |
| 232 | 14 | 9 | 3.08e−04 | 1,006 | −0.221 | 253 | 31 | 8.9 | 8.5 | 1 | 105 | 55 | 195 | 35 W |
| 232 | 13 | 9 | 3.23e−04 | 1,019 | 0.639 | 155 | 8 | 14.5 | | 1 | 40 | 72 | 130 | 18 S |
| 76 | 30 | 9 | 1.25e−04 | 1,032 | −0.014 | 334 | 5 | 11.2 | 6.8 | 1 | 233 | 68 | 323 | 22 E |
| 4 | 17 | 10 | 1.30e−04 | 1,016 | 0.565 | 15 | 21 | 17.1 | 5.5 | 1 | 194 | 69 | 284 | 21 N |
| 17 | 13 | 9 | 2.75e−04 | 1,008 | 0.126 | 38 | 2 | 12.5 | 4.8 | 1 | 133 | 72 | 223 | 18 W |
| 3 | 64 | 10 | 4.18e−04 | 1,011 | 0.321 | 256 | 24 | 17.2 | 12.8 | 1 | 31 | 57 | 121 | 33 S |
| 227 | 43 | 9 | 3.23e−04 | 1,015 | 0.208 | 181 | 21 | 10.9 | 3.8 | 1 | 45 | 62 | 135 | 28 W |
| 183 | 60 | 8 | 2.82e−04 | 1,019 | 0.831 | 319 | 7 | 22.3 | 6.8 | 1 | 181 | 81 | 271 | 9 N |
| 51 | 20 | 8 | 5.47e−04 | 1,051 | 0.431 | 7 | 8 | 10.2 | 3.9 | 1 | 244 | 75 | 334 | 15 E |
| 102 | 20 | 9 | 1.50e−03 | 1,047 | 0.602 | 204 | 15 | 21.6 | 7.2 | 1 | 330 | 66 | 60 | 24 S |
| 260 | 9 | 10 | 5.91e−03 | 1,006 | 0.272 | 117 | 16 | 9.4 | 4.7 | 1 | 330 | 71 | 60 | 19 S |
| 255 | 50 | 9 | 6.52e−03 | 1,057 | 0.697 | 123 | 22 | 12.4 | 10.5 | 1 | 270 | 65 | 0 | 25 E |
| 67 | 16 | 10 | 1.65e−03 | 1,039 | 0.131 | 149 | 12 | 3.1 | 1.8 | 1 | 291 | 75 | 21 | 15 E |
| 327 | 60 | 9 | 1.02e−03 | 1,022 | 0.299 | 122 | 9 | 19.5 | 8.0 | 1 | 268 | 80 | 358 | 10 E |
| 136 | 21 | 9 | 1.52e−04 | 1,005 | 0.004 | 202 | 43 | 22.3 | 11.8 | 1 | 298 | 6 | 28 | 84 E |
| 97 | 84 | 9 | 1.15e−03 | 1,006 | −0.054 | 132 | 41 | 20.1 | | 1 | 201 | 19 | 290 | 71 S |
| 22 | 14 | 10 | 1.55e−03 | 1,007 | −0.447 | 333 | 5 | 8.3 | 2.0 | 1 | 65 | 26 | 155 | 64 W |
| 296 | 60 | 9 | 7.17e−05 | 1,042 | −0.112 | 66 | 24 | 20.4 | 12.0 | 1 | 252 | 66 | 342 | 24 E |
| 13 | 56 | 9 | 1.93e−03 | 1,037 | 0.581 | 132 | 10 | 20.1 | | 1 | 2 | 59 | 92 | 31 S |
| 336 | 64 | 9 | 1.40e−03 | 1,032 | 0.463 | 147 | 25 | 10.5 | 5.0 | 1 | 335 | 65 | 65 | 25 S |
| 340 | 70 | 9 | 1.65e−04 | 1,022 | 0.502 | 151 | 14 | 38.2 | 7.4 | 2 | 272 | 64 | 2 | 26 E |
| 291 | 58 | 8 | 1.03e−03 | 1,073 | −0.138 | 230 | 28 | 7.3 | 1.5 | 1 | 112 | 41 | 202 | 49 W |
| | | 4 | 1.61e−04 | 1,018 | 0.600 | 121 | 6 | 8.6 | | 1 | 329 | 84 | 56 | 6 S |
| 31 | 15 | 8 | 1.29e−03 | 1,046 | 0.712 | 328 | 5 | 29.7 | 5.5 | 2 | 194 | 83 | 284 | 7 N |
| 296 | 82 | 8 | 7.73e−03 | 1,042 | 0.839 | 309 | 31 | 17.3 | 2.3 | 1 | 90 | 53 | 180 | 37 W |
| 276 | 10 | 7 | 1.79e−04 | 1,008 | 0.123 | 175 | 3 | 68.7 | 8.3 | 3 | 297 | 85 | 27 | 5 E |
| 68 | 89 | 8 | 2.85e−04 | 1,020 | 0.592 | 101 | 1 | 47.7 | 6.3 | 3 | 358 | 86 | 88 | 4 S |
| 56 | 74 | 8 | 6.45e−04 | 1,011 | −0.027 | 298 | 37 | 6.2 | 3.2 | 1 | 110 | 53 | 200 | 37 W |
| 9 | 58 | 8 | 1.65e−03 | 1,088 | 0.638 | 92 | 9 | 24.2 | 1.3 | 1 | 232 | 78 | 324 | 12 E |
| 79 | 34 | 9 | 5.19e−05 | 1,015 | 0.628 | 89 | 43 | 23.9 | 4.5 | 1 | 287 | 46 | 17 | 44 E |
| 176 | 53 | 8 | 6.57e−05 | 1,022 | −0.208 | 23 | 34 | 5.7 | 2.0 | 1 | 118 | 7 | 208 | 83 W |
| 125 | 20 | 9 | 1.97e−04 | 1,009 | 0.512 | 137 | 21 | 35.0 | 4.5 | 2 | 334 | 68 | 64 | 22 S |
| 176 | 30 | 10 | 2.52e−04 | 1,012 | 0.705 | 239 | 7 | 11.6 | 2.7 | 1 | 347 | 66 | 77 | 24 S |
| 198 | 48 | 7 | 1.29e−04 | 1,015 | −0.320 | 109 | 23 | 24.9 | 4.3 | 1 | 242 | 57 | 332 | 33 E |
| 2 | 12 | 9 | 1.19e−04 | 1,009 | 0.457 | 115 | 8 | 34.9 | 9.0 | 2 | 283 | 82 | 13 | 8 E |
| 62 | 54 | 11 | 2.36e−04 | 1,047 | −0.110 | 317 | 24 | 5.4 | 2.3 | 1 | 74 | 45 | 164 | 45 W |
| 322 | 30 | 8 | 2.99e−04 | 1,034 | −0.110 | 275 | 35 | 6.8 | 4.1 | 1 | 91 | 55 | 181 | 35 W |
| 348 | 42 | 8 | 2.27e−04 | 1,120 | 0.391 | 292 | 21 | 7.1 | 4.0 | 1 | 122 | 69 | 212 | 21 W |
| 12 | 71 | 7 | 2.74e−04 | 1,084 | 0.211 | 82 | 29 | 26.8 | 5.4 | 2 | 348 | 8 | 78 | 82 S |
| 1 | 54 | 9 | 3.08e−04 | 1,010 | 0.590 | 258 | 50 | 12.2 | 6.2 | 1 | 96 | 39 | 186 | 51 W |
| 250 | 43 | 9 | 3.34e−04 | 1,008 | 0.545 | 303 | 70 | 59.7 | 5.0 | 3 | 64 | 11 | 154 | 79 W |
| 77 | 37 | 10 | 1.86e−04 | 1,010 | 0.437 | 3 | 57 | 36.0 | 10.4 | 2 | 111 | 12 | 201 | 78 W |
| 246 | 27 | 9 | 4.15e−04 | 1,019 | 0.437 | 252 | 22 | 60.5 | 9.6 | 3 | 75 | 68 | 165 | 22 W |
| 135 | 37 | 9 | 2.88e−04 | 1,010 | 0.158 | 234 | 21 | 12.0 | 5.6 | 1 | 137 | 16 | 227 | 74 W |
| 188 | 61 | 10 | 1.22e−04 | 1,020 | 0.463 | 28 | 40 | 21.4 | 7.4 | 1 | 164 | 40 | 254 | 50 N |
| 13 | 27 | 9 | 1.86e−04 | 1,025 | 0.095 | 103 | 3 | 13.2 | 6.0 | 1 | 198 | 59 | 288 | 31 N |
| 114 | 46 | 9 | 1.44e−04 | 1,017 | 0.528 | 128 | 43 | 12.6 | 7.3 | 1 | 307 | 47 | 38 | 43 E |
| 77 | 16 | 11 | 1.86e−04 | 1,014 | 0.001 | 157 | 7 | 13.6 | 9.4 | 1 | 299 | 81 | 29 | 9 E |
| 332 | 17 | 11 | 8.48e−05 | 1,022 | 0.162 | 355 | 12 | 35.4 | 23.5 | 2 | 88 | 10 | 178 | 80 W |
| 206 | 84 | 9 | 9.06e−04 | 1,007 | 0.299 | 210 | 20 | 21.2 | 5.5 | 1 | 48 | 69 | 138 | 21 W |
| 215 | 83 | 8 | 1.53e−04 | 1,010 | −0.310 | 81 | 40 | 12.5 | 5.4 | 1 | 324 | 29 | 54 | 61 S |
| 248 | 76 | 9 | 2.78e−04 | 1,009 | 0.057 | 160 | 36 | 20.4 | 6.4 | 1 | 356 | 53 | 86 | 37 S |
| 91 | 82 | 6 | 1.36e−04 | 1,014 | 0.750 | 321 | 20 | 7.7 | 2.7 | 1 | 231 | 2 | 321 | 88 E |
| 333 | 68 | 8 | 2.81e−04 | 1,008 | 0.091 | 133 | 21 | 4.7 | | 1 | 321 | 68 | 50 | 22 E |
| 42 | 27 | 8 | 2.07e−04 | 1,033 | 0.554 | 344 | 15 | 13.2 | 2.9 | 1 | 227 | 60 | 317 | 30 E |
| 34 | 98 | 9 | 8.65e−04 | 1,012 | 0.144 | 320 | 75 | 23.1 | 11.3 | 1 | 100 | 12 | 190 | 78 W |
| 25 | 31 | 7 | 1.06e−04 | 1,005 | 0.265 | 35 | 13 | 18.0 | 7.8 | 1 | 304 | 7 | 34 | 83 E |
| 356 | 32 | 9 | 1.78e−04 | 1,013 | 0.445 | 298 | 29 | 13.8 | 5.5 | 1 | 156 | 55 | 246 | 35 N |
| 24 | 72 | 10 | 6.12e−04 | 1,003 | −0.069 | 309 | 16 | 31.6 | 9.2 | 2 | 201 | 50 | 291 | 40 N |
| 244 | 50 | 11 | 1.59e−04 | 1,006 | 0.542 | 303 | 45 | 17.8 | 5.5 | 1 | 164 | 37 | 254 | 53 N |
| 144 | 56 | 9 | 3.85e−04 | 1,019 | 0.196 | 246 | 5 | 20.0 | 13.0 | 1 | 144 | 67 | 237 | 24 N |
| 73 | 61 | 10 | 2.33e−03 | 1,027 | −0.035 | 135 | 38 | 22.5 | 9.0 | 1 | 356 | 44 | 86 | 46 S |

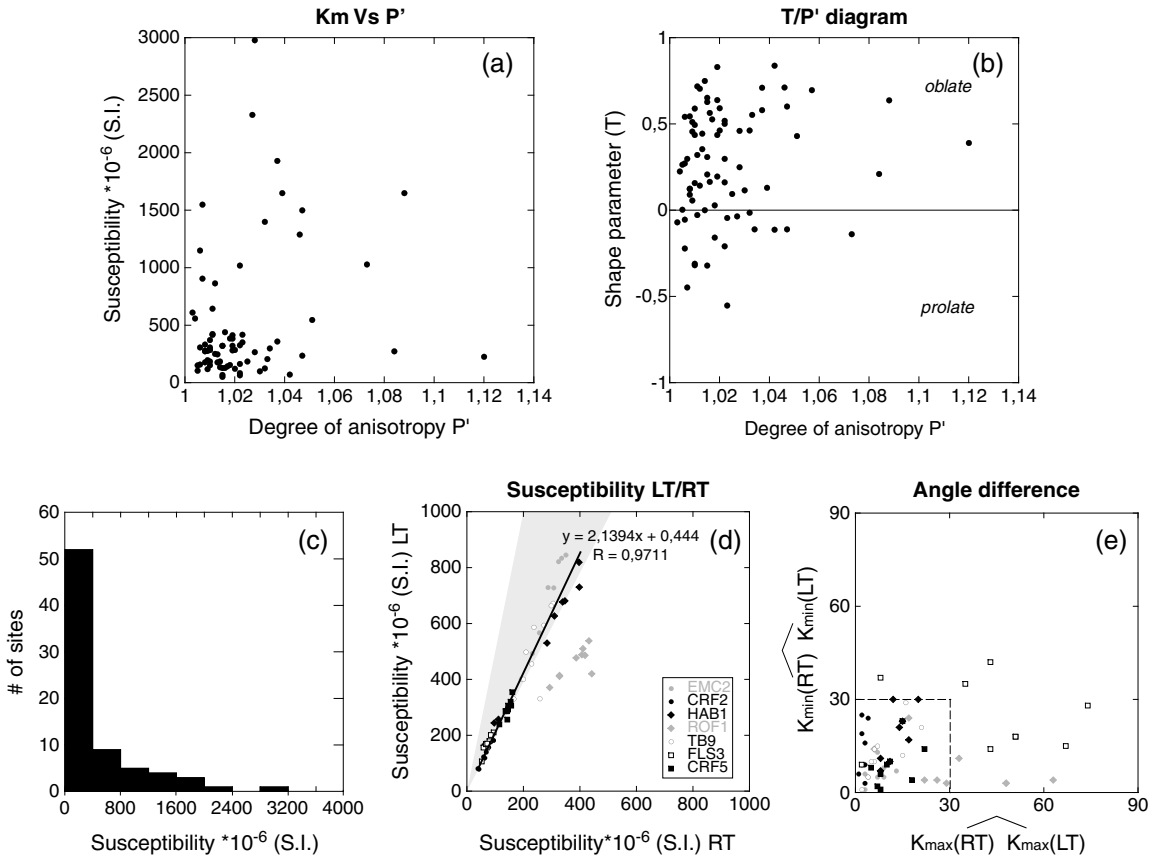


**Figure 7.** Scalar parameters of the room temperature magnetic fabric and low-temperature experiments. (a) Susceptibility (S.I.) versus corrected degree of anisotropy (*P'*) at the level of sites. (b) *T*/*P'* diagram showing the shape and the corrected anisotropy degree of magnetic ellipsoids, which are mainly oblate. (c) Histogram of bulk susceptibility versus number of sites. Most of the samples (73%) present low values, characteristic of the paramagnetic range. (d) Susceptibility of representative rock types analyzed at room and low temperatures, with relationships indicating their paramagnetic contribution. (e) Angles between $K_{max}$ measured at low and room temperatures as well as these angles measured for $K_{min}$. Note that sites ROF1 and FLS3 do not follow paramagnetic behavior.

The enhancement of paramagnetic fabric at low temperature (LT-AMS, 77 K) follows the Curie-Weiss law [*Parés and van der Pluijm*, 2002], and therefore, this method provides an estimation of the paramagnetic contribution to the magnetic anisotropy. The magnetic susceptibility in most samples that were cooled down to 77 K ($\kappa_{lt}$) increased by a factor of 2 with respect to that at the room temperature ($\kappa_{rt}$) (Figure 7d), mainly reflecting the subfabric associated with paramagnetic minerals. Only few samples maintained similar susceptibility values at low temperature, including site ROF1 (ignimbrite, Currabubula Formation, northern Tamworth Belt), two specimens from site HAB1 (sandstone, Byabarra Formation, East Hastings) and one specimen from site TB9 (greywacke, Baldwin Formation, northern Tamworth Belt). Considering all the data, the average $\kappa_{lt}/\kappa_{rt}$ ratio is 2.15. Low angular differences ($<$30°) between directions of $K_{max}$ and $K_{min}$ at low (77 K, LT) and room temperature (RT) are observed in most cases (Figure 7e), except for seven samples from site FLS3 (lavas, Isismurra Formation, Rouchel Block) and three samples from ROF1 (ignimbrite, Currabubula Formation, northern Tamworth Belt). As the Curie-Weiss law is valid only for paramagnetic materials [*Richter and van der Pluijm*, 1994], these results indicate that paramagnetic minerals dominate the AMS fabric in 74% of the 61 analyzed samples. Samples FLS3 and ROS1, which are volcaniclastic and acid volcanic rocks, respectively, show a high angular difference between $K_{max}$ ($K_{min}$) at LT and at RT and low $\kappa_{lt}/\kappa_{rt}$ ratio. The orientation of the principal axes is expected to be similar at LT and RT if paramagnetic minerals carry the susceptibility, whereas deviations from this similarity can occur due to diamagnetic or ferromagnetic contribution to the magnetic susceptibility.

### 4.2. Directional Data

Our results represent 10 structural domains: (1) Emu Creek-Mount Barney, (2) northern Tamworth Belt, (3) Rouchel, (4) Gresford, (5) Myall, (6) South Hastings, (7) West Hastings, (8) North Hastings, (9) NE Hastings, and

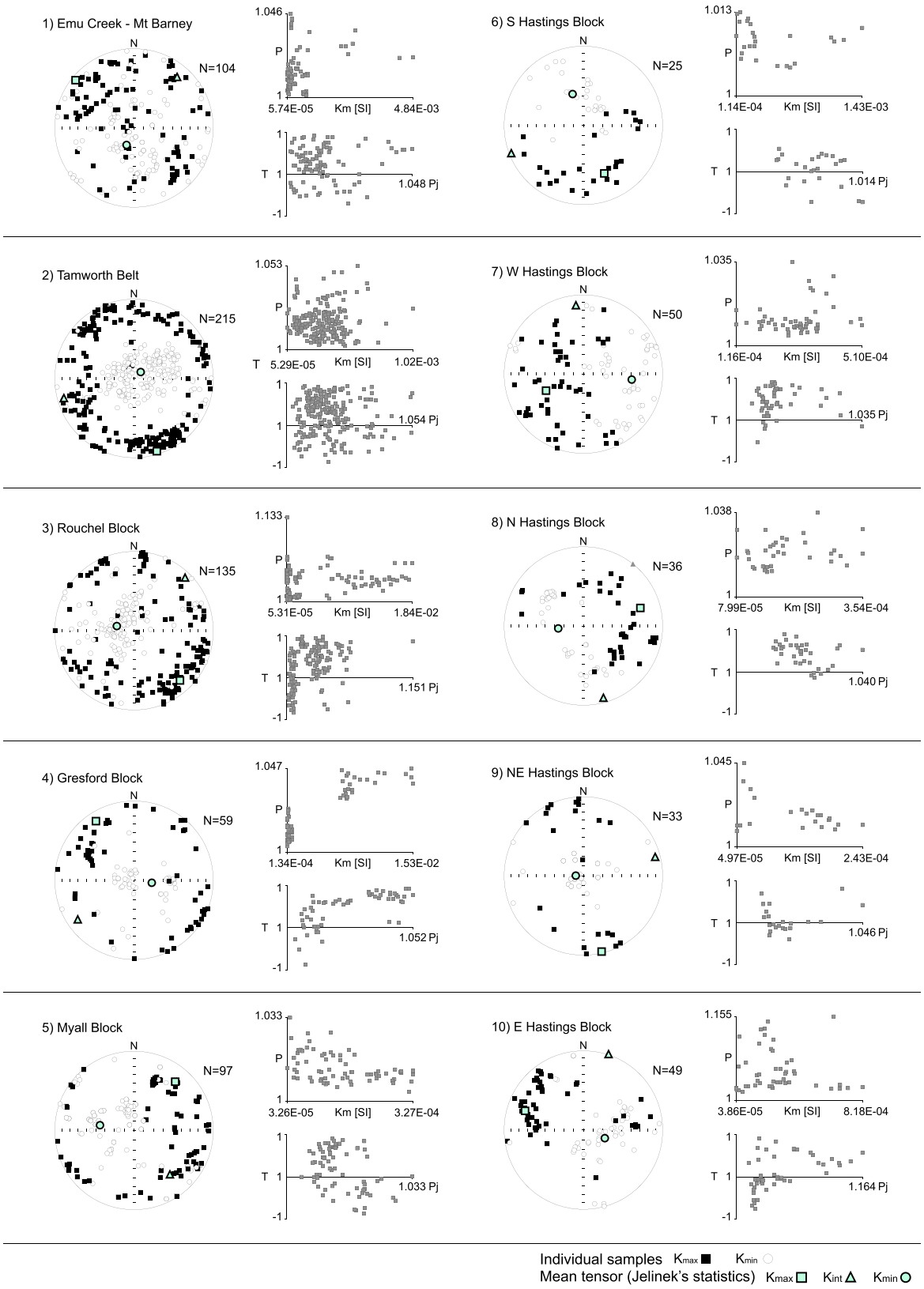


**Figure 8.** Stereoplots showing directional data of the complete collection of samples (geographic coordinate system, equal area, lower hemisphere, and 2% contour interval), mean tensor of lineations, and strike of the foliation planes. Susceptibility (Km) versus degree of anisotropy (*P*) diagrams. *T*/*P*′ diagram showing the shape and the corrected anisotropy degree of magnetic ellipsoids, which are mainly oblate ($T > 0$) but abundant prolate ellipsoids are also present ($T < 0$).

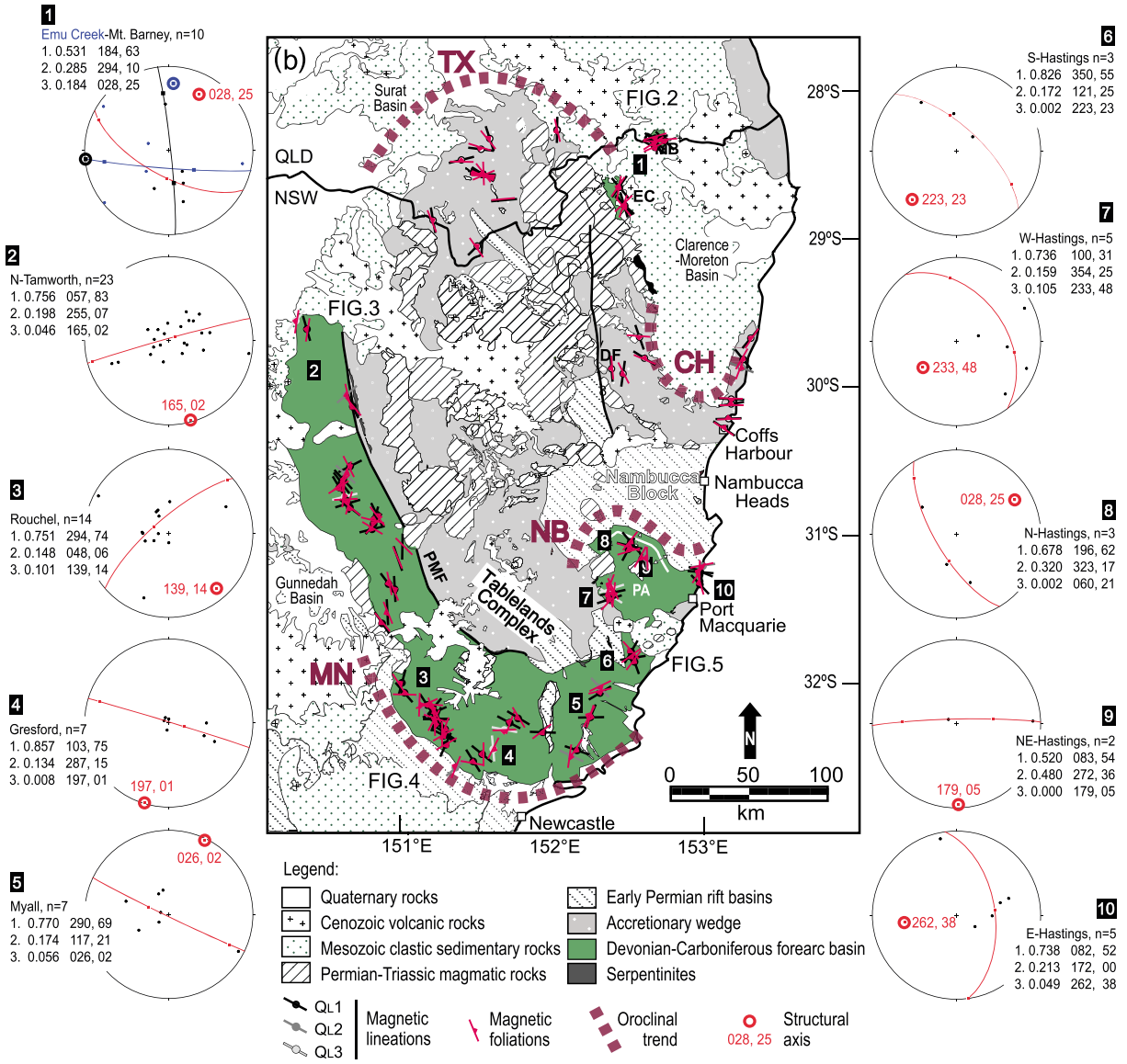


**Figure 9.** Map of the study area showing magnetic lineations ($Q_L1$) in black, $Q_L2$ in dark grey, $Q_L3$ in bright grey, and foliations in red, organized in structural domains. Data by *Aubourg et al.* [2004] are also shown following the same quality criteria. Stereoplots of $K_{min}$, eigenvalues, and eigenvectors (trend, plunge) are shown for each structural domain, with the girdle calculated using the Bingham statistics. Circles are poorly defined in plots 1, 3, 5, and 10. The pole to girdle is the local fold axis. Magnetic fabric lineations are filtered ($Q_L1$) and axes orthogonal to the girdle are shown in Figure 10.

(10) East Hastings. Directional data are presented in Figures 8 and 9 and Table 1. Magnetic lineations from all sites ($Q_L$) fall into three categories according to their half-confidence angles of $K_{max}$ within the $K_{max} - K_{int}$ plane ($E_{12}$) [*Martín-Hernández et al.*, 2004]. Well-defined magnetic lineations with $E_{12}$ angle of $<25°$ in rocks with paramagnetic predominance confirmed by low-temperature (LT) AMS analyses fall into the first group ($Q_L1$). They represent 78.5% of the sites (Table 1). Poorly defined lineations with $25° < E_{12} < 40°$, fall into the second group ($Q_L2$) and represent 13.9% of the sites. Undefined lineations with $E_{12} > 40°$, or those from rocks with nonparamagnetic dominance, fall into the third group ($Q_L3$) and represent 7.6% of the sites.

The stereoplots of the axes of the magnetic ellipsoids (Figure 8) show different orientations of the lineations (Jelinek's statistics) [*Jelinek*, 1981]. In Figure 9, only $Q_L1$ quality magnetic lineations are shown (in black), as well as foliations (in red). *Bingham* [1974] distributions of $K_{min}$, trending are orthogonal to the structural axes of the folds, are also shown in Figure 9, and the orientation of $K_{min}$ and structural axes are indicated next to

each stereoplot. All directional distributions in this study demonstrate either prolate or oblate fabric; no triaxial fabric has been found (Figure 9).

Trends of AMS lineations from the Emu Creek-Mount Barney region vary from 035° to 246°, with a mean value of 317° (see Table 1 and Figure 8). The distribution of $K_{min}$ is scattered and the Bingham fitting describes a structural axis at 028° (Figure 9), which is inconsistent with lineations. However, the structural axis combines two separate groups, one with an East-West (084°) trend in Mount Barney (black in Figure 9) and another with a North-South (004°) trend in Emu Creek (blue in Figure 9). This indicates that the two areas possibly belong to separate structural domains (see discussion below).

Eighty percent of the samples in the northern Tamworth Belt show NNW-SSE lineation trends with a mean value of 343° (ranging from 317° to 015°), but the rest demonstrate an orthogonal maximum value with a mean orientation of 242° (ranging from 218° to 256°), oblique to the main trend (Figure 8). The Bingham distribution provides a structural axis of 345° and concurs with the main NNW-SSE trend of lineations (Figure 9).

In the Rouchel Block, two major orientations of lineations can be distinguished. The most common trend (70% of samples) is 135° (varying from 117° to 153°). The second $K_{max}$ maximum (30% of samples) ranges from 187° to 246°, with a mean value of 209° (Figure 8). $K_{min}$ distribution encompasses a girdle with a structural axis at 319°, consistently with the mean lineation trends (Figure 9).

In the Gresford Block, only 25% of the lineations deviate from the average orientation of 303° (ranging from 298° to 309°, Figure 8). Foliations, determined as the axial plane of the WNW-ESE girdle distribution of $K_{min}$, show a 017° trend, which deviates from the main lineation trend (Figure 9).

The majority of the lineations in the Myall Block is characterized by an ENE-WSW trend, with a mean orientation of 076° (Figure 8). The structural axis, as determined by magnetic foliations, is 206° and is deflected with respect to the lineations (Figure 9).

Magnetic lineations and foliations in the Hastings Block are variable. The South Hastings sector shows scattered lineations with a main NNW-SSE orientation (average 159°, Figure 8). $K_{min}$ distribution defines a girdle with a structural axis at 043° (Figure 9). In the West Hastings sector, lineations are oriented NE-SW (244°, Figure 8). The structural axis shows a trend of 053° (Figure 9), which is orthogonal to the girdle defined by $K_{min}$ and is similar to the main lineation trend. In the North Hastings sector, lineations are moderately scattered and are oriented ENE-SSW (average 090°, Figure 8). The structural axis, determined from the $K_{min}$ distribution, is 060° (Figure 9). This orientation is inconsistent with lineations but surprisingly similar to the trend of the structural axes in the South and West Hastings sectors. In the NE Hastings sector, only few reliable data are available, but one lineation (157°, Figure 8) and structural axis (179°, orthogonal from $K_{min}$ girdle, Figure 9) are consistent with the general NNW-SSE trend. The East Hastings sector reveals ENE-WSW orientations (115° in average, Figure 8) and a structural axis that shows a somewhat similar orientation of 082° (orthogonal to $K_{min}$ girdle distribution, Figure 9).

## 5. Discussion

### 5.1. Comparison With Previous AMS Data

The only available AMS data from the NEO are those published by *Aubourg et al.* [2004] from the Texas and Coffs Harbour Oroclines. Unlike the data presented in our paper, *Aubourg et al.* [2004] studied Carboniferous rocks from the accretionary complex (Tablelands Complex) and the overlying early Permian sedimentary rocks.

The majority of the 28 sites studied by *Aubourg et al.* [2004] showed a good agreement between the magnetic fabric and the structural data. The authors linked the magnetic lineations and foliations to the pervasive structural fabrics developed within the accretionary wedge prior to oroclinal bending. A noticeable amplification in the degree of anisotropy and the steeply plunging magnetic lineations toward the hinges of the Texas and Coffs Harbour Oroclines led *Aubourg et al.* [2004] to suggest that the magnetic fabric was affected by a secondary imprint related to oroclinal deformation.

Data from *Aubourg et al.* [2004] are shown in Figure 9 and Table 2. We have applied our quality criteria ($Q_L$) for their lineations (Table 2). Sixty-three percent of the lineations show an East-West trend (283°, $\alpha_{95} = 12.5$), whereas the remaining 37% of the samples show a more scattered distribution with an average North-South

AGU Tectonics

10.1002/2013TC003483

**Table 2.** Field Data and Magnetic Fabric Parameters From *Aubourg et al.* [2004], Including Site Locations and Quality of Lineations ($Q_L$) and Foliations

| Site | Longitude (°)E | Latitude (°)S | *N*# | So Dip Az (deg) | So Dip (deg) | S1 Dip Az (deg) | S1 Dip (deg) | $K_{max}$ Dec (deg) | $K_{max}$ Inc (deg) | $a_{95}$ | $Q_L$ | $K_{min}$ Dec (deg) | $K_{min}$ Inc (deg) | Foliation (Pole From K3) Dec (deg) | Foliation (Pole From K3) Inc (deg) DD | Lithology |
|---|---|---|---|---|---|---|---|---|---|---|---|---|---|---|---|---|
| ATTA | 151.43 | 28.98 | 13 | 280 | 20 | 225 | 25 | 45 | 63 | 7 | 1 | 235 | 27 | 325 | 63 E | Silicified shale |
| ATTB | 151.15 | 28.81 | 9 | 252 | 27 | | | 350 | 49 | 8 | 1 | 248 | 10 | 338 | 80 E | Silicified shale |
| ATTC | 151.33 | 28.39 | 13 | 170 | 5 | 180 | 5 | 76 | 64 | 13 | 1 | 181 | 7 | 271 | 83 n | Sandstone, siltstone |
| ATTD | 151.48 | 28.32 | 12 | | | 188 | 0 | 277 | 83 | 16 | 1 | 17 | 1 | 107 | 89 S | Silicified shale |
| ATTE | 151.53 | 28.26 | 12 | 252 | 50 | 218 | 47 | 342 | 39 | 21 | 1 | 231 | 23 | 321 | 67 E | Mudstone |
| ATTF | 151.98 | 28.21 | 14 | | | 50 | 25 | 181 | 31 | 5 | 1 | 77 | 22 | 167 | 68 W | Sandstone, siltstone |
| ATTN | 151.6 | 28.67 | 12 | 336 | 5 | 180 | 5 | 265 | 5 | 10 | 1 | 355 | 4 | 85 | 86 S | Silicified shale |
| ATCK | 152.55 | 29.58 | 12 | 18 | 32 | | | 161 | 31 | 8 | 1 | 4 | 57 | 94 | 33 S | Silicified shale |
| ATCL | 152.58 | 29.75 | 13 | 242 | 16 | | | 302 | 43 | 8 | 1 | 203 | 9 | 293 | 81 n | Massive sandstone |
| ATCI | 152.43 | 29.86 | 10 | | | 238 | 10 | 188 | 84 | 11 | 1 | 63 | 4 | 153 | 86 W | Shale |
| ATCJ | 152.35 | 29.84 | 15 | 237 | 26 | 80 | 10 | 355 | 635 | 7 | 1 | 85 | 1 | 175 | 89 W | Siltstone |
| ATCE | 153.14 | 30.21 | 10 | 222 | 2 | | | 304 | 15 | 17 | 1 | 214 | 1 | 304 | 89 n | Mudstone |
| ATCD | 153.19 | 30.18 | 9 | 192 | 14 | | | 88 | 6 | 17 | 1 | 178 | 1 | 268 | 89 n | Mudstone |
| ATCC | 153.2 | 30.08 | 8 | 192 | 20 | 170 | 5 | 81 | 26 | 7 | 1 | 180 | 17 | 270 | 73 n | Mudstone |
| ATCB | 153.2 | 30.06 | 13 | 185 | 26 | 180 | 20 | 93 | 9 | 3 | 1 | 2 | 7 | 92 | 83 S | Siltstone, mudstone |
| ATCF | 153.29 | 29.82 | 12 | 280 | 10 | | | 112 | 55 | 33 | 2 | 291 | 35 | 21 | 55 E | Mudstone |
| ATCH | 153.3 | 29.78 | 13 | 286 | 36 | 350 | 5 | 141 | 63 | 21 | 1 | 300 | 25 | 30 | 65 E | Mudstone |
| ATCG | 153.34 | 29.61 | 13 | 110 | 24 | | | 220 | 9 | 13 | 1 | 124 | 34 | 214 | 56 W | Siltstone, mudstone |
| ATTO | 151.48 | 28.51 | 13 | 197 | 71 | | | 96 | 4 | 4 | 1 | 188 | 34 | 278 | 56 n | Mudstone |
| CTTA | 151.48 | 28.51 | 10 | 207 | 36 | | | 291 | 7 | 22 | 1 | 52 | 78 | 142 | 12 W | Siltstone, mudstone |
| CTTB | 151.48 | 28.51 | 10 | 198 | 45 | | | 298 | 6 | 4 | 1 | 198 | 56 | 288 | 34 n | Sandstone, mudstone |
| CTTC | 151.48 | 28.51 | 10 | 200 | 50 | | | 303 | 12 | 4 | 1 | 157 | 75 | 247 | 15 n | Sandstone |
| CTTD | 151.48 | 28.51 | 11 | 203 | 59 | | | 297 | 1 | 4 | 1 | 204 | 67 | 294 | 23 n | Mudstone |
| CTTE | 151.48 | 28.51 | 10 | 13 | 69 | | | 283 | 1 | 6 | 1 | 189 | 67 | 279 | 23 n | Mudstone |
| CTTF | 151.48 | 28.51 | 9 | | 90 | | | 284 | 2 | 5 | 1 | 193 | 14 | 283 | 76 n | Mudstone |
| CTTG | 151.48 | 28.51 | 7 | 192 | 74 | | | 284 | 5 | 5 | 1 | 193 | 10 | 283 | 80 n | Mudstone |
| CTTH | 151.48 | 28.51 | 8 | 196 | 74 | | | 271 | 3 | 5 | 1 | 181 | 0 | 271 | 90 n | Mudstone |
| ATCA | 152.29 | 28.92 | 12 | 40 | 70 | | | 352 | 5 | 4 | 1 | 88 | 53 | 178 | 37 W | Mudstone |

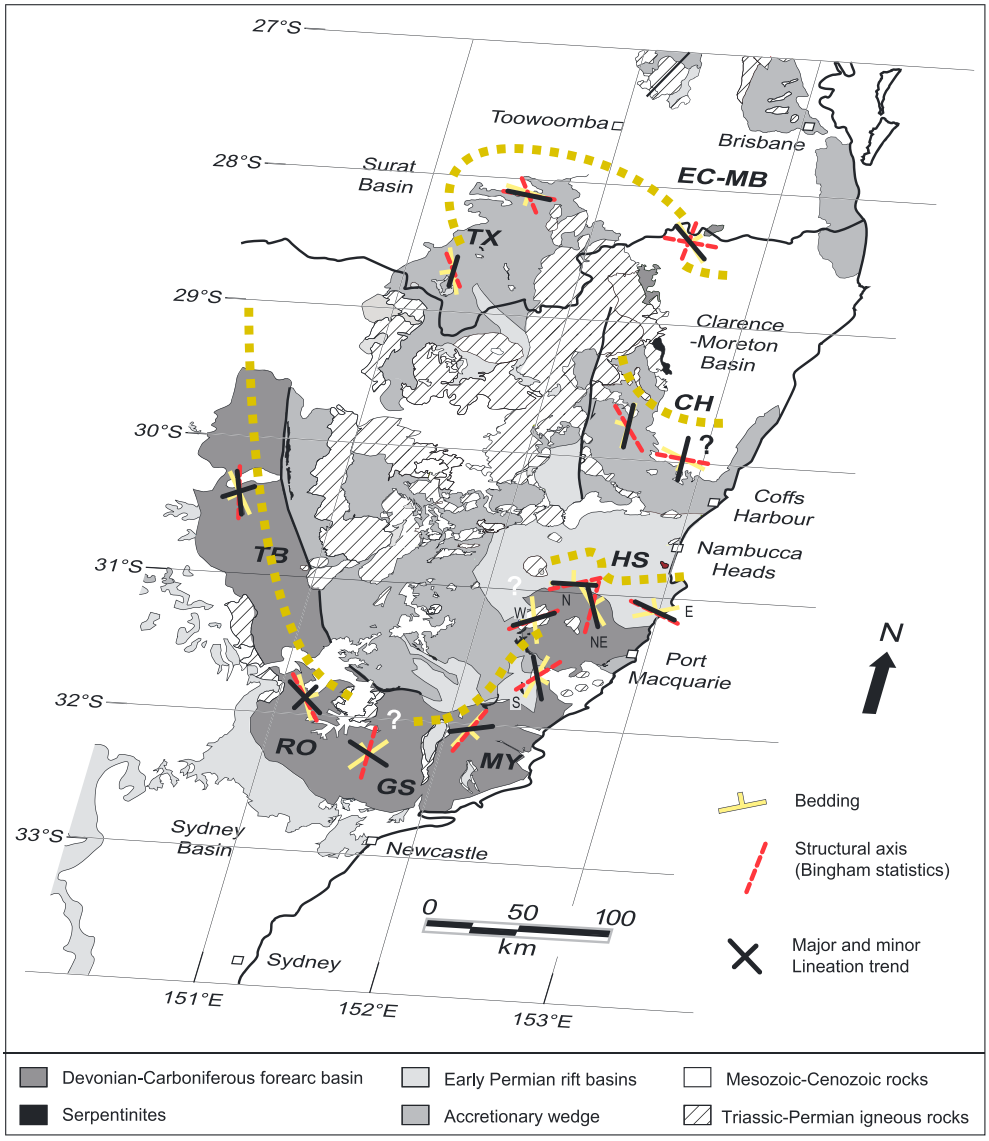


**Figure 10.** Major and minor statistic representation of magnetic lineation trends and structural axes in the southern NEO. Note inconsistent orientations in the southern Coffs Harbour Orocline, Gresford Block, and South and West Hastings sectors. The other structural domains show consistency between structural and magnetic patterns, supporting the existence of the Manning and Nambucca (Hastings) Oroclines. Structural domains are CH, Coffs Harbour; EM-MB, Emu Creek-Mount Barney; TX, Texas; TB, northern Tamworth Belt; RO, Rouchel; GS, Gresford; MY, Myall; HS, Hastings.

orientation (179°, $\alpha_{95} = 32.2$). The analysis of the Bingham distribution of $K_{min}$ shows that 60% of the structural axis orientations are East-West (098°), with the remaining 40% of the samples showing an approximately North-South (170°) orientation. Therefore, these data show a reasonable consistency between the AMS data and the structure of the Texas and Coffs Harbour Oroclines, with approximately East-West orientations clustered at the hinges of the oroclines and approximately North-South orientations at the limbs.

### 5.2. Relationships Between AMS Data and the New England Oroclines

Figure 10 shows a comparison of bedding orientations and all reliable AMS data ($Q_L1$), including the tensorial means of major and minor lineations and structural axes obtained from the $K_{min}$ Bingham distribution. As mentioned in the previous section, data from *Aubourg et al.* [2004] are consistent with the structure of the Texas and Coffs Harbour Oroclines [*Korsch and Harrington*, 1987; *Murray et al.*, 1987; *Lennox and Flood*, 1997; *Offler and Foster*, 2008; *Cawood and Leitch*, 1985; *Glen and Roberts*, 2012; *Li et al.*, 2012]. In the area of

these oroclines, there is also a relatively good agreement between the orientations of lineations, structural axis, and bedding, except for the southern part of the Coffs Harbour Orocline, where the structural axis and bedding are almost identical but orthogonal to the magnetic lineation (Figure 10). This could be attributed to noncoaxial deformation, which can deflect the lineation with respect the structural trend or to the superposition of a later deformation on an early East-West fabric in the southern Coffs Harbour Orocline [*Korsch*, 1978].

Our data from the Emu Creek Block and Mount Barney inlier (eastern limb of the Texas Orocline) show a similarity between bedding and lineation, but a slight deviation from the structural axis determined from the $K_{min}$ Bingham distribution, which is oriented approximately North-South in Emu Creek and approximately East-West in Mount Barney (blue and black in stereoplot 1, Figure 9). A combined stereoplot representation shows a structural axis of 028°, defined by a rather scattered $K_{min}$ distribution (Figure 9). We propose that the two localities do not represent the same structure. Rather, the Emu Creek and Mount Barney inliers possibly correspond to the limb and hinge of the Coffs Harbour Orocline, respectively. This suggestion, however, remains speculative due to the scarcity of structural information from the Mount Barney area. The aeromagnetic image from this area shows a NW-SE structural grain in the Emu Creek Block (dashed lines in Figure 6b), which is consistent with observations [*Hoy et al.*, 2014], but the structural grain in Mount Barney is masked by high magnetic anomalies associated with Cenozoic basalts (Figure 6b).

In the northern Tamworth Belt, the orientations of the lineations and structural axes determined from the $K_{min}$ Bingham distribution are consistent (Figure 10). In contrast, bedding orientations are slightly inconsistent with the AMS data, but local bedding measurements are scattered due to low dips despite of the overall NNW-SSE structural pattern (Figure 3). This confirms that AMS is a powerful tool for evaluating strain axes. A minor group of subhorizontal foliations fits with the Bingham adjustment of $K_{min}$ axes (Figure 9, stereoplot 2). Cleavage orientations range from N-S to NW-SE, parallel to the major structures in the northern Tamworth Belt (e.g., Peel Fault and Mooki Thrust). Bedding, magnetic lineations, and structural axes show similar orientations to these structures. The general NNW-SSE trend of the magnetic fabric in this domain is consistent with the expected strain in this segment of the belt, as well as with the superposition of approximately East-West contraction associated with the Hunter-Bowen phase of deformation. Magnetic lineations with minor oblique trends (EES-WWN) may have resulted from a component of noncoaxial deformation.

In the Rouchel Block, 70% of the AMS data show a SW-NE orientation, approximately parallel to the observed cleavage (sites GVG1, CGV10, and FLS3), but the remaining 30% show a fabric perpendicular to it. The average bedding orientation is parallel to the major SE-NW structural trend (Figure 10), which could be related to the western limb of the Manning Orocline. North-South orientations may correspond to a superimposed East-West contraction associated with the Hunter-Bowen deformation, whereas oblique fabrics are possibly linked to noncoaxial deformation.

In the Gresford Block, there is only limited coincidence between the magnetic lineation and bedding (East-West), and a structural axis with a North-South orientation, which makes difficult to draw conclusions on the structural pattern (Figure 10). The orientations of magnetic lineations may follow the hinge of the Manning Orocline. In contrast, the structural axis and bedding show an orthogonal orientation that could be linked to approximately East-West Hunter-Bowen contraction.

The Myall Block shows a relatively good consistency between magnetic and structural indicators. The structural axis determined from the $K_{min}$ Bingham distribution and bedding seems to coincide with the NNE-SSW trend, which is consistent with the orientation at the eastern limb of the Manning Orocline. However, lineations are deviated to an East-West orientation, possibly due to the effect of approximately East-West Hunter-Bowen contraction.

The Hastings Block revealed the most complex pattern of magnetic fabrics. In the South Hastings, both lineations and beddings have a North-South orientation, whereas the structural axis is NE-SW. Bedding in West Hastings is oriented NNW-SSE, but lineations and structural axis determined from the $K_{min}$ Bingham distribution show an ENE-WSW trend. This inconsistency could be related to multidirectional deformational stages recorded in the magnetic fabric. Magnetic fabrics in the North Hastings and NE Hastings are oriented East-West and SSE-NNW, respectively. These orientations of lineation, structural axis and bedding are consistent with the expected expression of the Parrabel anticline (Figure 5). The East Hastings sector shows an ENE-WSW trend of bedding, whereas magnetic fabric shows an ESE-WNW pattern.

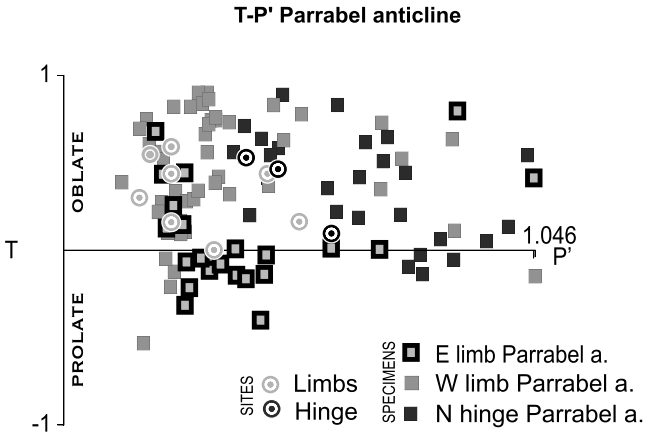


**Figure 11.** Diagram showing relationships between the shape (*T*) and the corrected degree of anisotropy (*P'*) for the Parrabel anticline (Hastings Block). Note that samples from the hinge of the anticline show a higher degree of magnetic anisotropy.

With the exception of the West Hastings sector, the overall pattern of magnetic fabrics in the Hastings Block is generally consistent with the shape of the Nambucca Orocline and its more local expression of the Parrabel anticline. This is supported by bedding orientations that folded around a great circle with a fold axis oriented NW-SE, which is the same direction as the fold axis for the orocline. Our analysis of the magnetic fabric in 15 sites around the Parrabel anticline shows a consistent occurrence of a coherent magnetic lineation with locally observed bedding azimuths (Figure 10). Scalar parameters studied for the Parrabel anticline, indicate a higher degree of anisotropy in the hinge areas, indicating higher strain in comparison to the limbs. The shape of the ellipsoid does not show differences between hinge and limbs, except the eastern limb that reveals a prolate shape (Figure 11).

Figure 12 shows individual $K_{max}$ and $K_{min}$ axes of the magnetic ellipsoid from each site, and the mean lineation and structural axis for each macrostructural domain. We define four macrostructural domains, including (1) the eastern limb of the Texas Orocline (Emu Creek-Mount Barney), (2) western limbs of the Texas and Manning Oroclines (northern Tamworth Belt), (3) hinge of the Manning Orocline (Rouchel, Gresford, and Myall Blocks), and (4) the eastern limb of Manning Orocline, including the Nambucca Orocline (Hastings Block). We first plotted in situ (Figures 12, 1) and tilt corrected (Figures 12, 2) $K_{max}$ and $K_{min}$ orientations and then applied an "orocline correction" (Figures 12, 3a) for each macrostructural domain, assuming an original North-South orientation and a complete oroclinal behavior. In addition, we applied "paleomagnetic correction" (Figures 12, 3b) based on published paleomagnetic interpretations for vertical-axis block rotations, which include 120° clockwise rotation of the eastern limb of the Texas Orocline [*Aubourg et al*., 2004], 80° counterclockwise rotation of the Rouchel and Gresford Blocks [*Geeve et al*., 2002], 120° counterclockwise rotation of the Myall Block [*Geeve et al*., 2002], and 130° counterclockwise rotation of the Hastings Block [*Schmidt et al*., 1994].

Figure 12 shows that for the Texas Orocline (Emu Creek-Mount Barney) and Manning Orocline (Rouchel, Gresford, and Myall Blocks), there is a relatively good agreement between the oroclinal and paleomagnetic corrections, indicated by approximately similar orientations of $K_{max}$ means. Nevertheless, the results from the Hastings Block are inconsistent, showing a contrast between approximately North-South and approximately East-West orientations of $K_{max}$ in the oroclinal correction and paleomagnetic correction, respectively. This suggests that the Hastings Block underwent a different kinematic history with respect to the Tamworth Belt, or that available paleomagnetic data are not representative of the original trend (e.g., due subsequent remagnetizations). It can also suggest that the Hastings Block did not behave as a rigid block and that higher resolution data are needed in order to properly unravel its kinematic history. Overall, the structural axes determined by AMS are in agreement with the structural trends of the Texas, Manning, and Nambucca/Hastings Oroclines and provide a useful tool to determine the degree of relationship between deformational strain markers and the complex oroclinal structure of the NEO. This result is in agreement with recent suggestions on the complex quadruple oroclinal structure of the southern NEO [*Rosenbaum*, 2010; *Glen and Roberts*, 2012; *Rosenbaum*, 2012b; *Rosenbaum et al*., 2012]. We emphasize, however, that the AMS data can only provide information on the finite strain associated with the oroclines. As such, our data likely represent an imprint of multideformational stages in NEO, possibly associated with an early phase of oroclinal bending in the early Permian that was followed by the Late Permian to Triassic Hunter-Bowen phase of deformation. Further constraints on the timing and magnitude of block rotations require a detailed paleomagnetic study and cannot be obtained by AMS data.

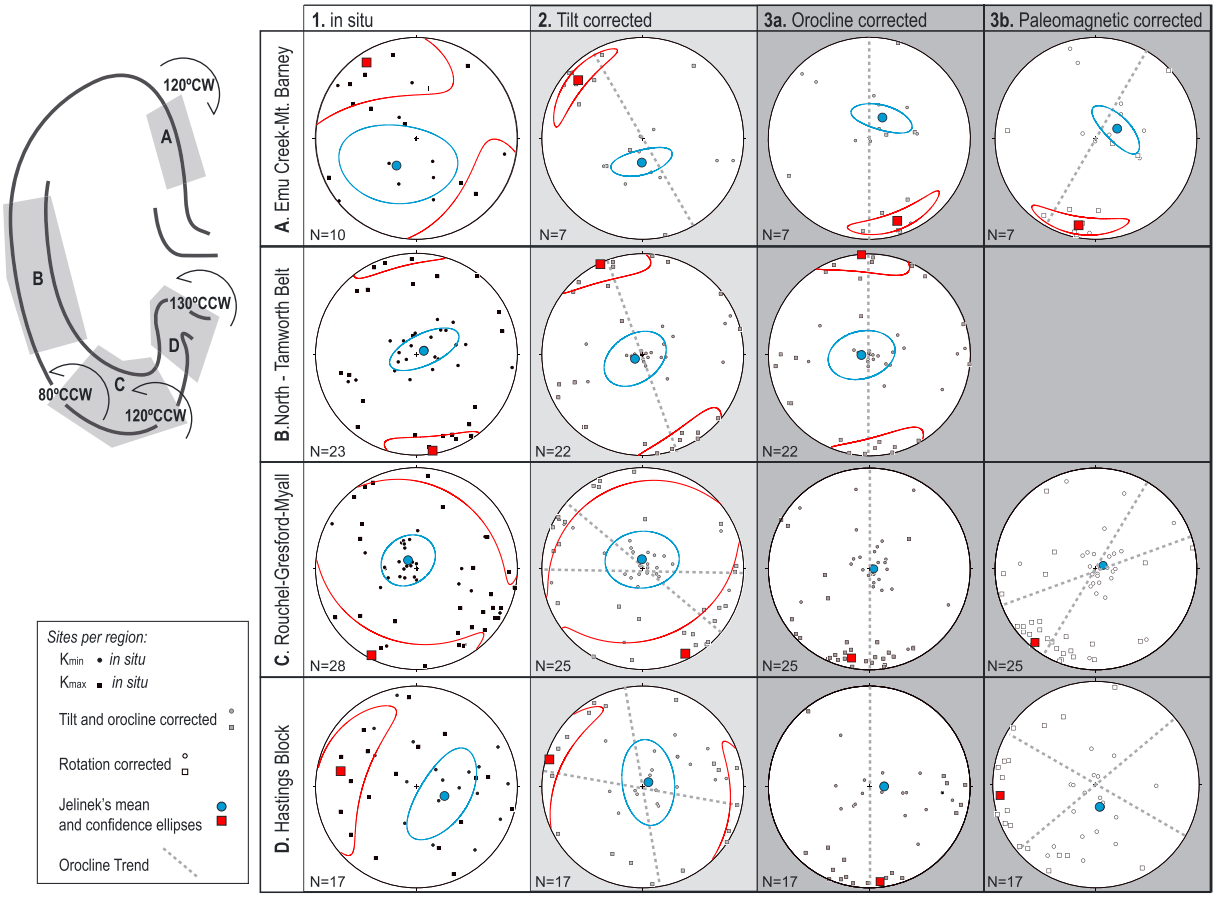


**Figure 12.** Reconstruction of the magnetic fabric in four macrostructural domains. Equal area stereoplots of $K_{min}$ and $K_{max}$ of the sites and Jelinek's means per macrostructural domain [*Jelinek*, 1981] are shown. (1) In situ data, (2) tilt corrected (*N*# of sites depending of bedding availability), (3a) orocline-corrected, and (3b) paleomagnetic corrected orientations. Differential reconstruction of the oroclinal bending (Figures 12, 3a) and paleomagnetic data (Figures 12, 3b) does not allow calculating confidence ellipses for Rouchel-Gresford-Myall and Hastings macrostructural domains.

### 5.3. Suborthogonal Magnetic Fabrics

We suggest that there is a link between the magnetic fabric and the complex deformation of the NEO oroclines, with the trends of the magnetic lineation (and commonly also the structural axis) parallel to the structures. However, in most of the structural domains, we also recognize secondary magnetic fabric features, with lineation suborthogonal to the main orogenic trend. This is most evident in the northern Tamworth, Rouchel, Gresford, and West Hastings domains.

In order to understand the origin of oblique or suborthogonal magnetic features, we conducted petrographic investigation on representative samples. The exposed Devonian-Carboniferous fore-arc basin rocks in the NEO have been subjected to burial metamorphism produced at zeolite and prehnite-pumpellyite facies conditions [*Offler et al.*, 1997]. However, our petrographic observations show no evidence for metamorphism. Bedding-parallel stylolitic planes appear in some sites, such as BYA3 (Byabarra Formation, South Hastings) and LOW2 (Lowana Formation, northern Tamworth Belt). We therefore discard metamorphism as the source of secondary magnetic fabrics.

Suborthogonal magnetic fabrics can be caused by sedimentation environments, as confirmed by the petrographic observations of the involved samples. Specimens with suborthogonal fabrics from the northern Tamworth Belt and Rouchel Block mainly consist of coarse-grained lithologies (sandstone) with sedimentary structures, such as cross-bedding stratification or convolutes, that probably deflected magnetic fabrics from the main trend. Some of the sites from the data set are associated with oblate fabrics where magnetic lineation is less resolved (northern Tamworth Belt, Myall Block) or related to sharp prolate ellipsoids where magnetic foliation is difficult to define (Hastings Block).

Alternatively, the suborthogonal fabric could arise from various tectonic processes. For example, shearing along foliation planes could have scattered the orientation of the magnetic lineation. This deformation could have happened, for example, during the Hunter-Bowen phase. Another hypothesis is that oroclinal bending partially reset previous deformation, and the orthogonal magnetic lineations are in fact linked to an early orogen-orthogonal extensional phase.

## 6. Conclusions

Magnetic fabric investigation in the southern NEO reveals that AMS is mainly carried by paramagnetic minerals, implying that the magnetic and crystallographic fabrics are comparable. The magnetic fabric mimics bedding and cleavage orientation and allows us to define the shape of the oroclines. These results confirm that AMS can help unraveling structural fabrics when field evidence is unclear. This is best demonstrated in the structural grains of the northern Tamworth Belt and in the Parrabel anticline (Hastings Block), which are clearly defined by the magnetic fabric.

We show that the structural axis, which we define as orthogonal to the Bingham's distribution of $K_{min}$ in a structural domain, is an efficient tool for defining the orientation of a set of linear components of the magnetic fabric, especially when these components are shallowly plunging. We find a good agreement between local structural directions and magnetic lineations along the oroclines. When considering also available paleomagnetic data, we recognize in the back-rotated magnetic lineations an original approximately NE-SW orogenic system (Figures 12, 3b). Structural and AMS consistency is not observed in the Hastings Block, where additional high-resolution data are needed to unravel its associated block rotations and to build paleogeographic reconstruction.

**Acknowledgments**

This work was funded by an ARC Discovery grant (DP130100130). T.M. was granted with a FIRB-Abruzzo contract. We are very grateful to Antonio Casas (UZ) and the Geotranfer Research Group funds (CGL2009-08969) for providing support during the AMS analyses. We thank Abbas Babaahmadi for assisting with aeromagnetic interpretation, Uri Shaanan for fieldwork support, and Nathan Siddle for sample preparation. This is contribution 495 from the ARC Centre of Excellence for Core to Crust Fluid Systems (http://www.ccfs.mq.edu.au) and TIGeR publication #584. The manuscript benefited from the comments by the journal's reviewers, Charles Aubourg and two anonymous reviewers. The data for this paper are available by contacting the corresponding author (taniamochales@gmail.com).

## References

Aitchison, J. C., P. G. Flood, and F. C. P. Spiller (1992), Tectonic setting and paleoenvironment of terranes in the southern New England orogen, eastern Australia as constrained by radiolarian biostratigraphy, *Palaeogeogr. Palaeoclimatol. Palaeoecol.*, *94*, 31–54.

Aitchison, J. C., M. C. J. Blake, P. G. Flood, and P. G. Jayko (1994), Paleozoic ophiolitic assemblages within the southern New England orogen of eastern Australia: Implications for growth of the Gondwana margin, *Tectonics*, *13*(5), 1135–1149, doi:10.1029/93TC03550.

Aubourg, C., C. Klootwijk, and R. J. Korsch (2004), Magnetic fabric constraints on oroclinal bending of the Texas and Coffs Harbour Blocks: New England Orogen, eastern Australia, in *Magnetic Fabric: Methods and Applications*, edited by F. Martín-Hernández et al., *Geol. Soc., London Spec. Publ.*, 421–445.

Aubourg, C., B. Smith, A. Eshraghi, O. Lacombe, C. Authemayou, K. Amrouch, O. Bellier, and F. Mouthereau (2010), New magnetic fabric data and their comparison with paleostress markers in the Western Fars Arc (Zagros, Iran): Tectonic implications, in *Tectonic and Stratigraphic Evolution of Zagros and Makran During the Mesozoic–Cenozoic*, edited by C. Robin and P. Leturmy, *Geol. Soc. London Spec. Publ.*, *330*, 97–120.

Bingham, C. (1974), An antipodally symmetric distribution on the sphere, *Annales of Statistics*, *2*, 1201–1225.

Binns, R. A., et al. (1967), *Geological Map of New England, 1:250,000—New England Tableland, Southern Part, With Explanatory Text*, The Univ., of New England, Armidale.

Blake, M. C., and B. L. Murchey (1988), A California model for the New England Fold Belt, in *New England Orogen: Tectonics and Metallogenesis*, edited by J. D. Kleeman, pp. 20–31, Univ. of New England, Armidale, Australia.

Borradaile, G. (1988), Magnetic susceptibility, petrofabrics and strain, *Tectonophysics*, *156*, 1–20.

Bouchez, J. L. (1997), Granite is never isotropic: An introduction to AMS studies of granitic rocks, in *Granite: From Segregation of Melt to Emplacement Fabrics*, edited by J. L. Bouchez, D. H. W. Hutton, and W. E. Stephens, pp. 95–112, Kluwer Acad., Dordrecht, Netherlands.

Brown, R. E., J. P. Krynen, and J. W. Brownlow (1992), *Manilla-Narrabri 1:250 000 Metallogenic Map*, 1st ed., Geol. Surv. of New South Wales, Sydney.

Capitanio, F. A., C. Faccenna, S. Zlotnik, and D. R. Stegman (2011a), Subduction dynamics and the origin of Andean orogeny and the Bolivian orocline, *Nature*, *480*(7375), 83–86.

Carey, S. W. (1955), The orocline concept in geotectonics, *Pap. Proc. R. Soc. Tasmania*, *89*, 255–288.

Cawood, P. A. (1982), Structural relations in the subduction complex of the Paleozoic New England fold belt, eastern Australia, *J. Geol.*, *90*(4), 381–392.

Cawood, P. A. (2005), Terra Australis Orogen: Rodinia breakup and development of the Pacific and Iapetus margins of Gondwana during the Neoproterozoic and Paleozoic, *Earth Sci. Rev.*, *69*, 249–279.

Cawood, P. A., and E. C. Leitch (1985), Accretion and dispersal tectonics of the Southern New England Fold Belt, Eastern Australia, in *Tectonostratigraphic Terranes of the Circum-Pacific Region*, *Earth Sci. Ser.*, edited by D. G. Howell, pp. 481–492, Circum-Pacific Council for Energy and Mineral Resources, Houston, Tex.

Cawood, P. A., S. A. Pisarevsky, and E. C. Leitch (2011a), Unravelling the New England orocline, east Gondwana accretionary margin, *Tectonics*, *30*, TC5002, doi:10.1029/2011TC002864.

Cawood, P. A., E. C. Leitch, R. Merle, and A. A. Nemchin (2011b), Orogenesis without collision: Stabilizing the Terra Australis accretionary orogen, eastern Australia, *Geol. Soc. Am. Bull.*, doi:10.1130/B30415.1.

Cifelli, F., M. Mattei, and F. Rossetti (2007), The tectonic evolution of arcuate mountain belts on top of a retreating subduction slab: The example of the Calabrian Arc, *J. Geophys. Res.*, *112*, B09101, doi:10.1029/2006JB004848.

Collins, W. J. (1991), A re-assessment of the "Hunter-Bowen Orogeny": Tectonic implications for the southern New England Fold Belt, *Aust. J. Earth Sci.*, *38*, 409–423.

Craven, S. J., N. R. Daczko, and J. A. Halpin (2012), Thermal gradient and timing of high-T-low-P metamorphism in the Wongwibinda Metamorphic Complex, southern New England Orogen, Australia, *J. Metamorph. Geol.*, *30*, 3–20.

Cross, K. C., C. L. Fergusson, and P. G. Flood (1987), Contrasting structural styles in the Paleozoic subduction complex of the Southern New England Orogen, Eastern Australia, in *Terrane Accretion and Orogenic Belts*, *Geodyn. Ser.*, edited by E. Leitch and E. Scheibner, pp. 83–92, AGU, Washington D. C.

Dirks, P. H. G. M., M. Hand, W. J. Collins, and R. Offler (1992), Structural-metamorphic evolution of the Tia complex, New England fold belt; thermal overprint of an accretion-subduction complex in a compressional back-arc setting, *J. Struct. Geol.*, *14*(6), 669–688.

Flood, P. G., and J. C. Aitchison (1992), Late Devonian accretion of the Gamilaroi terrane to Gondwana: Provenance linkage provided by quartzite clasts in the overlap sequence, *Aust. J. Earth Sci.*, *39*, 539–544.

Geeve, R. J., P. W. Schmidt, and J. Roberts (2002), Paleomagnetic results indicate pre-Permian counter-clockwise rotation of the southern Tamworth Belt, southern New England Orogen, Australia, *J. Geophys. Res.*, *107*(B9), 2196, doi:10.1029/2000JB000037.

Gilligan, L. B., J. W. Brownlow, and R. G. Cameron (1987), *Tamworth-Hastings 1:250 000 Metallogenic Map*, 1st ed., Geol. Surv. of New South Wales, Sydney.

Glen, R. A. (2005), The Tasmanides of eastern Australia, in *Terrane Processes at the Margins of Gondwana*, edited by A. P. M. Vaughan, P. T. Leat, and R. J. Pankhurst, *Geol. Soc. London Spec. Publ.*, *246*, 23–96.

Glen, R. A., and J. Roberts (2012), Formation of oroclines in the New England Orogen, eastern Australia, *J. Virtual Explorer*, *43*, Paper 3, doi:10.3809/jvirtex.2012.00305.

Graham, J. W. (1966), Significance of magnetic anisotropy in Appalachian sedimentary rocks, in *The Earth Beneath the Continents*, *Geophys. Monogr. Ser.*., vol. 10, edited by J. S. Steinhart and T. J. Smith, pp. 627–648, AGU, Washington D. C.

Holcombe, R. J., C. J. Stephens, C. R. Fielding, D. Gust, T. A. Little, R. Sliwa, J. Kassan, J. McPhie, and A. Ewart (1997), Tectonic evolution of the northern New England Fold Belt: The Permian Triassic Hunter-Bowen event, in *Tectonics and Metallogenesis of the New England Orogen: Alan Voisey Memorial Volume*, edited by P. M. Ashley and P. G. Flood, *Geol. Soc. Australia Spec. Publ.*, *19*, 52–65.

Housen, B., and B. A. van der Pluijm (1991), Slaty cleavage development and magnetic anisotropy fabrics, *J. Geophys. Res.*, *96*, 9937–9946, doi:10.1029/91JB00605.

Hoy, D., G. Rosenbaum, R. Wormald, and U. Shaanan (2014), Geology and geochronology of the Emu Creek Block (northern New South Wales, Australia) and implications for oroclinal bending in the New England Orogen, *Aust. J. Earth Sci.*, in press.

Hrouda, F. (1982), Magnetic anisotropy of rocks and its application in geologyç and geophysics, *Geophys. Surv.*, *5*, 37–82.

Jelinek, V. (1981), Characterization of the magnetic fabric of rocks, *Tectonophysics*, *79*, 63–70.

Johnston, S. T., A. B. Weil, and G. Gutiérrez-Alonso (2013), Oroclines: Thick and thin, *Geol. Soc. Am. Bull.*, *125*(5–6), 643–663, doi:10.1130/B30765.1.

Klootwijk, C. (2009), Sedimentary basins of eastern Australia: Paleomagnetic constraints on geodynamic evolution in a global context, *Aust. J. Earth Sci.*, *56*(3), 273–308.

Klootwijk, C. T., and J. Giddings (1993), Paleomagnetic results of Upper Paleozoic volcanic, northeastern Queensland, and Australia's Late Paleozoic APWP, in *New England Orogen, Eastern Australia*, edited by P. G. Flood and J. C. Aitchison, pp. 617–627, Univ. of New England, Armidale, Australia.

Klootwijk, C. T., J. Giddings, and P. Percival (1993), *Paleomagnetic Reconnaissance of Upper Paleozoic Volcanics*, Australian Geological Survey Organization Record, 1993/36, Northeastern Queensland.

Korsch, R. J. (1978), Regional-scale thermal metamorphism overprinting low-grade regional metamorphism, Coifs Harbour Block, northern New South Wales, *J. Proc. R. Soc. N. S. W.*, *111*, 89–96.

Korsch, R. J. (1981), Deformational history of the Coffs Harbour Block, *J. Proc. R. Soc. N. S. W.*, *114*, 17–22.

Korsch, R. J., and H. J. Harrington (1987), *Oroclinal Bending, Fragmentation and Deformation of Terranes in the New England Orogen, Eastern Australia*, *Geodyn. Ser.*, vol. 19, pp. 129–139, AGU, Washington D. C., doi:10.1029/GD019p0129.

Korsch, R. J., J. M. Totterdell, T. Fomin, and M. G. Nicoll (2009), Contractional structures and deformational events in the Bowen, Gunnedah and Surat Basins, eastern Australia, *Aust. J. Earth Sci.*, *56*, 477–499.

Leitch, E. C. (1974), The geological development of the southern part of the New England Fold Belt, *J. Geol. Soc. Aust.*, *21*, 133–156.

Leitch, E. C. (1980), The Great Serpentine Belt of New South Wales: Diverse mafic–ultramafic complexes set in a Palaeozoic arc, in *Ophiolites: Proceedings, International Ophiolite Symposium, Cyprus*, Ministry of Agriculture and Natural Resources, edited by A. Panayitou, pp. 637–648, Geol. Surv. Department, Nicosia.

Lennox, P. G., and P. G. Flood (1997), Age and structural characterisation of the Texas megafold, southern New England Orogen, eastern Australia, in *Tectonics and Metallogenesis of the New England Orogen*, edited by P. M. Ashley and P. G. Flood, Geol. Soc. Spec. Publ., Australia, 161–177.

Lennox, P. G., and J. Roberts (1988), The Hastings Block, a key to the tectonic development of the New England Orogen, in *Conference on NEO-Tectonics and Metallogenesis, Dept. Geol. Geophys.*, edited by J. D. Kleeman, pp. 68–77, Univ. of New England, Armidale, Australia.

Lennox, P. G., R. Offler, and J. Yan (2013), Discussion of Glen R.A. and Roberts J. 2012: Formation of oroclines in the New England orogen, eastern Australia. In: Oroclines (Eds.) Stephen Johnston and Gideon Rosenbaum, *J. Virtual Explorer*, *43*, paper 3, 44.

Li, P., and G. Rosenbaum (2014a), Does the Manning Orocline exist? New structural evidence from the inner hinge of the Manning Orocline in the Armidale-Walcha area (eastern Australia), *Gondwana Res.*, *25*, 1599–1613.

Li, P., and G. Rosenbaum (2014b), Reply to comment by Offler et al. on "Does the Manning Orocline exist? New structural evidence from the inner hinge of the Manning Orocline (eastern Australia)," *Gondwana Res.*, in press.

Li, P., G. Rosenbaum, and P. J. T. Donchak (2012), Structural evolution of the Texas Orocline, eastern Australia, *Gondwana Res.*, *22*, 279–289.

Li, P., G. Rosenbaum, and P. M. Vasconcelos (2014), Chronological constraints on the Permian geodynamic evolution of eastern Australia, *Tectonophysics*, *617*, 20–30.

Lowrie, W., and A. M. Hirt (1987), Anisotropy of magnetic susceptibility in the Scaglia Rossa pelagic limestone, *Earth Planet. Sci. Lett.*, *82*, 349–356.

Marshak, S. (2004), Salients, recesses, arcs, oroclines, and syntaxes: A review of ideas concerning the formation of map-view curves in fold-thrust belts, in *Thrust Tectonics and Hydrocarbon Systems*, edited by K. R. McClay, *Am. Assoc. Pet. Geol.*, *82*, 131–156.

Martín-Hernández, F., C. M. Luneburg, C. Aubourg, and M. Jackson (2004), Magnetic fabric: Methods and applications—An introduction, in *Magnetic Fabric: Methods and Applications*, edited by F. Martín-Hernández et al., *Geol. Soc. London Spec. Publ.*, *238*, 1–7.

McElhinny, M. W., C. M. A. Powell, and S. A. Pisarevsky (2003), Paleozoic terranes of eastern Australia and the drift history of Gondwana, *Tectonophysics*, *362*, 41–65.

Murray, C. G., G. R. McClung, W. G. Whitaker, and P. R. Degeling (1981), Geology of Late Palaeozoic sequences at Mount Barney, Queensland and Paddys Flat, New South Wales, *Queensl. Gov. Min. J.*, *82*(955), 203–213.

Murray, C. G., C. L. Ferguson, P. G. Floood, W. G. Whitaker, and R. J. Korsch (1987), Plate tectonic model for the Carboniferous evolution of the New England Fold Belt, *Aust. J. Earth Sci.*, *34*, 213–236.
Nagata, T. (1961), *Rock Magnetism*, 2nd ed., pp. 350, Maruzen Company, Tokyo.
Offenberg, A. C. (1971), *Tamworth 1:250 000 Geological Sheet SH/56-13*, 1st ed., Geol. Surv. of New South Wales, Sydney.
Offler, R., and D. A. Foster (2008), Timing and development of oroclines in the southern New England Orogen, New South Wales, *Aust. J. Earth Sci.: Int. Geosci. J. Geol. Soc. Aust.*, *55*(3), 331–340.
Offler, R., and A. Williams (1987), Evidence for sinistral movement on the Peel Fault System in serpentinites, Glenrock Station, N.S.W, in *Terrane Accretion and Orogenic Belts, Geodyn. Ser.*, vol. 19, edited by E. C. Leitch and E. Scheibner, pp. 141–151, AGU, Washington D. C.
Offler, R., J. Roberts, P. G. Lennox, and J. Gibson (1997), Metamorphism in Palaeozoic forearc sequences, southern New England Fold Belt, NSW, Australia, in *Proceedings of the 30th International Geological Congress*, vol. 17, edited by Q. Xiangling et al., pp. 241–250, Precambrian Geology & Metamorphic Petrology, Beijing.
Offler, R., P. G. Lennox, G. Phillips, and J. Yan (2014), Comment on: "Does the Manning Orocline exist? New structural evidence from the inner hinge of the Manning Orocline (eastern Australia)" by Li and Rosenbaum (2013), *Gondwana Res.*, doi:10.1016/j.gr.2014.03.003, in press.
Parés, J. M., and B. A. van der Pluijm (2002), Evaluating magnetic lineations (AMS) in deformed rocks, *Tectonophysics*, *350*(4), 283–298.
Powell, C. M. A., Z. X. Li, and G. A. Thrupp (1990), Australian Palaeozoic palaeomagnetism and tectonics-I. Tectonostratigraphic terrane constraints from the Tasman Fold Belt, *J. Struct. Geol.*, *12*, 553–565.
Richter, C., and B. A. van der Pluijm (1994), Separation of paramagnetic and ferrimagnetic susceptibilities using low-temperature magnetic susceptibilities and comparison with high field methods, *Phys. Earth Planet. Inter.*, *82*, 113–123.
Roberts, J., and B. A. Engel (1987), Depositional and tectonic history of the southern New England Orogen, *Aust. J. Earth Sci.*, *34*, 1–20.
Roberts, J., P. G. Lennox, and R. Offler (1993), The geological development of the Hastings Block—Displaced fore-arc fragment of the Tamworth Belt, in *New England Orogen, Eastern Australia*, *Dep. Geol. Geophys.*, edited by P. G. Flood and J. C. Aitchison, pp. 231–242, Univ. of New England, Armidale, Australia.
Roberts, J., E. C. Leitch, P. G. Lennox, and R. Offler (1995), Devonian-Carboniferous stratigraphy of the southern Hastings Block, New England Orogen, eastern Australia, *Aust. J. Earth Sci.*, *42*, 609–633.
Rochette, P. (1987), Magnetic susceptibility of the rock matrix related to magnetic fabric studies, *J. Struct. Geol.*, *9*, 1015–1020.
Rochette, P., M. Jackson, and C. Aubourg (1992), Rock magnetism and the interpretation of anisotropy of magnetic susceptibility, *Rev. Geophys.*, *30*, 209–226, doi:10.1029/92RG00733.
Rosenbaum, G. (2010), Structure of the New England oroclines, in *New England Orogen 2010 Conference Proceedings*, edited by S. Buckman and P. L. Blevin, pp. 297–302, Univ. of New England.
Rosenbaum, G. (2012a), Oroclinal Bending in the southern New England Orogen (eastern Australia): A geological field excursion from Brisbane to Sydney, *J. Virtual Explorer*, doi:10.3809/jvirtex.2012.00311.
Rosenbaum, G. (2012b), Oroclines of the southern New England Orogen, eastern Australia, *Episodes*, *35*, 187–194.
Rosenbaum, G. (2014), Geodynamics of oroclinal bending: Insights from the Mediterranean, *J. Geodyn.*, doi:10.1016/j.jog.2014.05.002, in press.
Rosenbaum, G., and G. S. Lister (2004), Formation of arcuate orogenic belts in the western Mediterranean region, in *Orogenic Curvature: Integrating Paleomagnetic and Structural Analyses*, edited by A. J. Sussman and A. B. Weil, Geol. Soc. Am. Spec. Pap., 41–56, Boulder, Colo.
Rosenbaum, G., P. Li, and D. Rubatto (2012), The contorted New England Orogen (eastern Australia): New evidence from U-Pb geochronology of Early Permian granitoids, *Tectonics*, *31*, TC1006, doi:10.1029/2011TC002960.
Sagnotti, L., F. Speranza, A. Winkler, M. Mattei, and R. Funiciello (1998), Magnetic fabric of clay sediments from the external northern Apennines (Italy), *Phys. Earth Planet. Inter.*, *105*, 73–93.
Scheibner, E. (1976), *Explanatory Notes on the Tectonic Map of New South Wales*, pp. 283, Geol. Surv. of New South Wales, Sydney.
Schmidt, P. W., C. Aubourg, P. G. Lennox, and J. Roberts (1994), Palaeomagnetism and tectonic rotation of the Hastings Terrane, eastern Australia, *Aust. J. Earth Sci.*, *41*(6), 547–560.
Shaanan, U., G. Rosenbaum, P. Li, and P. M. Vasconcelos (2014), Structural evolution of the early Permian Nambucca Block (New England Orogen, eastern Australia) and implications for oroclinal bending, *Tectonics*, *33*, 1425–1443, doi:10.1002/2013TC003426.
Shaw, S. E., and R. H. Flood (1981), The New England batholith, eastern Australia: Geochemical variations in time and space, *J. Geophys. Res.*, *86*, 10,530–44, doi:10.1029/JB086iB11p10530.
Speranza, F., L. Sagnotti, and M. Mattei (1997), Tectonics of the Umbria–Marche–Romagna Arc (central–northern Apennines, Italy): New paleomagnetic constrains, *J. Geophys. Res.*, *102*, 3153–3166, doi:10.1029/96JB03116.
Stephenson, N. C. N., and H. D. Hensel (1982), Amphibolites and related rocks from the Wongwibinda metamorphic complex, northern N.S. W., Australia, *Lithos*, *15*, 59–75.
Stroud, W. J., and R. E. Brown (1998), *Inverell 1:250 000 Metallogenic Map*, 1st ed., Geol. Surv. of New South Wales, Sydney.
Sussman, A. J., and A. B. Weil (2004), Preface, in *Orogenic Curvature: Integrating Paleomagnetic and Structural Analyses*, edited by A. J. Sussman and A. B. Weil, *Geol. Soc. Am. Spec. Pap.*, *383*, v–vii.
Van der Voo, R. (2004), Paleomagnetism, oroclines, and growth of the continental crust, *GSA Today*, *14*, 4–9.
Wartenberg, W., R. J. Korsch, and A. Schäfer (2003), The Tamworth Belt in Southern Queensland, Australia: Thrust-characterized geometry concealed by Surat Basin sediments, in *Tracing Tectonic Deformation Using the Sedimentary Record*, edited by T. McCann and A. Saintot, *Geol. Soc. London Spec. Publ.*, *208*, 185–203.
Wellman, P. (1990), A tectonic interpretation of the gravity and magnetic anomalies in southern Queensland, *Aust. Bur. Miner. Resour. Bull.*, *232*, 21–34.
Whitaker, W. G., P. M. Green, and R. W. Stephens (1980), *Moreton Geology 1:500 000 Geological Map, Queensland*, Dep. of Mines, Brisbane, Australia.
Yonkee, A., and A. B. Weil (2010), Reconstructing the kinematic evolution of curved mountain belts: Internal strain patterns in the Wyoming salient, Sevier thrust belt, U.S.A., *Geol. Soc. Am. Bull.*, *122*(1–2), 24–49, doi:10.1130/B26484.1.